PERUVIAN NAZCA TRIDACYTLS:

Comparative anatomy between hominids (M-type) and reptilian (J-type) tridactyls

A scientific study using CT scan with advanced 3D image reconstruction and virtual dissection.

By ***Dr. K .H. Fung*** *(Hong Kong SAR, China) June 2026*

ACKNOWLEDGEMENT

- The author wished to thank Tridactyls.org for granting permission to use the DICOM CT datasets available on their website for this scientific study.

SECTION 1: WHAT ARE BEING STUDIED?

- The term 'Tridactyls'(tri=3 dactyls=digits) refers to dessicated corpses and remains first discovered in 2015 in cave or underground tunnel system in the Peruvian desert near Nazca. They all share common feature of bipedalism bearing 3 digits in hands and feet.

- M-type tridactyls are the group of bipedal tridactyl specimens referred to as 'hominids' showing strong resemblance to human but otherwise possess some odd and unusual features not found in modern humans. M-type tridactyls nicknamed '***Maria***', '***Montserrat***' (including her baby '***Rafael***') and a child nicknamed '***Sebastian***' are included in the current study. (*Figure 1*)

- J-type tridactyls are the group of bipedal tridactyl specimens referred to as 'reptilians'. They are smaller than the M-type, roughly about 60 cm in length. They bear anatomical features entirely different from human. Perhaps the only significant common feature they share with the M-type is again the hallmark presence of 3 fingers and 3 toes. J-type tridactyls nicknamed '***Josefina***','***Luisa***' and '***Alberto***' are included in the current study. *(Figure 2)*

- Anatomical and factual comparison will be made between the 2 groups. The study will be conducted using advanced 3D image reconstruction and digital virtual dissection based on the original publicly available DICOM CT datasets obtained with permission from Tridactyls.org. (https://tridactyls.org)

SECTION 1: WHAT ARE BEING STUDIED? (contd.)

- Computed tomography (CT) is an advanced non-invasive digital imaging technique that made use of X-ray to provide a collection of serial cross-sectional images, achieving sub-millimetre resolution with current equipments. Furthermore, the image datasets can be input into advance 3D imaging computer software (e.g. *Osirix, Weasis*) for further manipulation, providing not only multi-planar 2D sectional images in any planes but also 3D images, including cinematic display and virtual reality/virtual endoscopy display options. Specific bone and organs can be digitally segmented using direct volume rendering or shaded-surface-display to generate 3D imageries. False colouring of the digital model helps to enhance visual impact. 3D mesh models can also be exported to create correctly sized scaled physical models using 3D printing.

- Any introduced human artefacts (including most sutural materials, metal or plastic inserts), tool marks on bones, bone fixation devices, extraneous implanted bones etc. can be easily identified employing CT scanning with 3D reconstruction due to differences in densities (Hounsfield CT units), orientation, alignment, congruity of matching bone surfaces, proportion, size and shape etc. particularly when compare with known human data. CT scanning is a known documentation technique capable of confirming authenticity and in ruling out artificial manipulation.

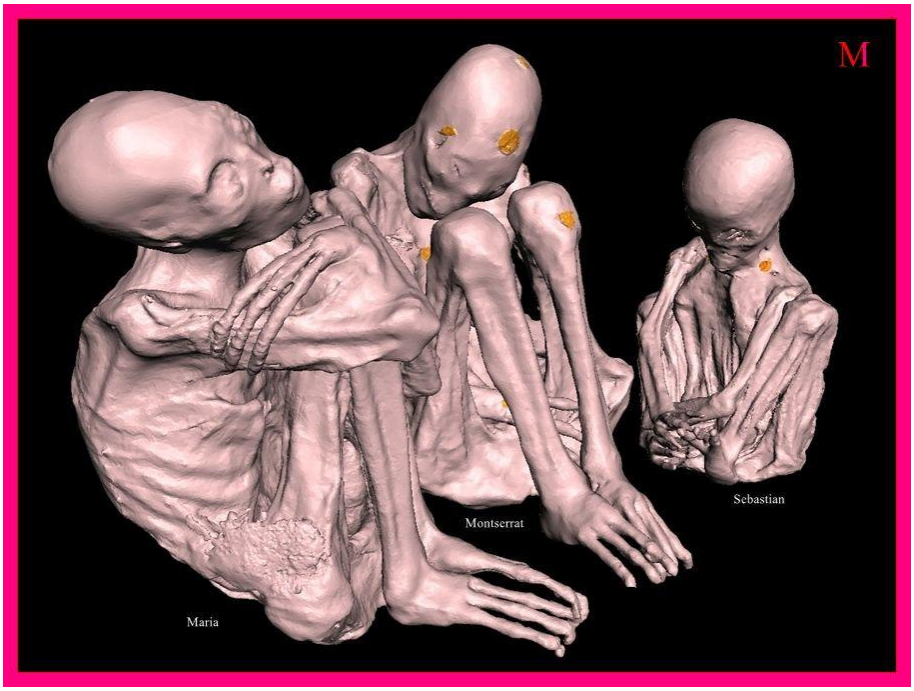

Figure 1: 3D CT showing comparative sizes and external morphology of M-type triadactyls *(from left to right)* '***Maria***', '***Montserrat***' and a child '***Sebastian***'. Locations of implants *(in gold colour)* in '***Montserrat***' and '***Sebastian***' are visible.

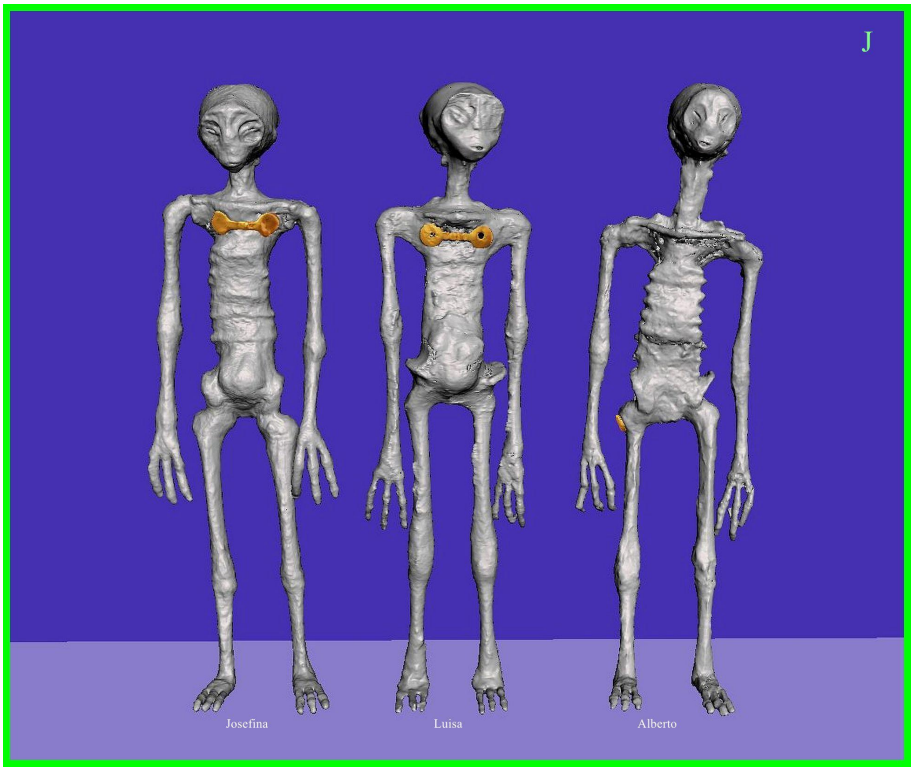

Figure 2: 3D CT showing comparative size and external morphology of J-type triadactyls *(from left to right)* '***Josefina***', '***Luisa***' and '***Alberto***'. Locations of implants *(in gold colour)* are visible. Note the disproportionally long neck in '***Alberto***'. Body & joint structures and even limb proportions differ significantly from human or 'M-type" tridactyls.

SECTION 2: PRESERVATION STATUS

M-type tridactyls:

• The M-type tridactyls are complete dessicated corpses of difficult sizes and ages including adults and children. *(Figure 1)* They are preserved in a fine white powder identified as diatomaceous earth (DE). The powder is normally beyond the resolution of CT scan (unless in large conglomerate clumps) thus allowing for a clear view of the skin surface. *(Figure 3)* Breast can be found in '***Maria***' and '***Monserrat***'. No evidence of navel could be identified in all tridactyls.

•The bodies are very well preserved with intact external and internal organs including skin, teeth, bones, muscles, ligaments, tendons and fascia.

•Internal organs including outlines of trachea, bronchi, heart chambers and blood vessels can be identified.

•All contain remnant shrunken brain tissues within the skull. *(Figures 4,25)*

•Solid organs e.g. liver and spleen are replaced by air but leaving behind their capsules. However, pancreas and kidneys could not be identified.

•Abundant bowel content including coprolites with ingested intact seeds can be found.

•Metallic implants are found in '***Maria***' '***Montserrat***'& '***Sebastian***'. The subcutaneous implants in *'**Montserrat**'* showed soft tissue overgrowth. The neck implant in *'**Sebastian**'* stimulated significant bone overgrowth. *(Figures 5,6.7)*

•Evidence of major soft tissue and bone injuries including fractures are found in '***Maria***', '***Montserrat***' and '***Sebastian***'. Large haematoma can be identified. Disruption of Achilles tendons can be found in '***Maria***'.

•Evidence of diseases including bone degeneration and multiple osteolytic bone metastases from tumour are found in '***Maria'***. *(Figure 57)*

•'***Montserrat***' is pregnant containing a well-formed humanoid foetus '***Rafael***'. *(Figures 8,39)*

•Overall, the anatomy was found to be well structured, anatomically coherent, complex, natural and could not have been due to artificial construct. No suture material nor artificial bone fixation device were found.

SECTION 2: PRESERVATION STATUS (contd.)

J-type tridactyls:

- All J-type tridactyls studied are very well-preserved complete dessicated corpses of similar sizes (roughly about 60 cm) but showing individual variations. All are smaller than and morphologically different internally and externally from the M-type tridactyls. *(Figure 2)*

•All are dessicated corpses with white powdery covering of diatomaceous earth (DE) that is not normally visible on CT, hence allowing for a clear view of the skin surface.

•The skin surfaces remain intact. After computer enhancement to improve resolution of the 3D image, bristle-like projections can be found on the scalp of '***Josefina***'. Also reptile-like patterned skin texture can also be seen in the scalp and in the face of *'**Josefina**'*. *(Figure 9)* No navel nor nipple could be identified on CT.

•The J-type tridactyls under study adopt a straight rigid posture with extended upper and lower limbs. The odd and unreal look due to the rigid posture in J-type tridactyls had made skeptics to dismiss them immediately as hoax without further study. However, such posture could be explainable if after dessication and when placed in an extended posture, the skin can became tough and contracted down onto the bones, behaving like a shrink wrap. In fact, different degree of shrinkage are noticeable in the studied tridactyls. *(Figure 10)*

•Strong external compression force could also have been applied on the gastralia to cause random ribs to be broken and found penetrating into the spinal canal through intervertebral foramen in all 3 tridactyls. Scattered compression fractures in spine and prolapsed intervertebral disks can also be found. *(Figure 11)*

•Bilateral shoulders are found to have dislocated upwards in '***Josefina***' and *'**Luisa**'*. In addition, extensive haematoma is noted in bilateral arm pits of *'**Luisa**'*. *(Figure 12)*

•'***Josefina***' and '***Luisa***' are found bearing large eggs with hyper-dense content in their right side of their bulging pelvic abdomen. '***Alberto***' was found without eggs. *(Figures 2,11,13,43,44)*

•Remnants of shrunken brain tissue are found inside the skulls of '***Josefina***' and '***Alberto***'. *(Figures 4,21,59)*

•2 sophisticated dumb bell-shaped metallic implants are found below the furcula in '***Josefina***' and '***Luisa***'. A notched roundish disk-like metallic implanted located over right hip of '***Alberto***' could have been related to bone healing following injury to the underlying upper femoral epiphysis. *(Figures 2, 14,15,16)*

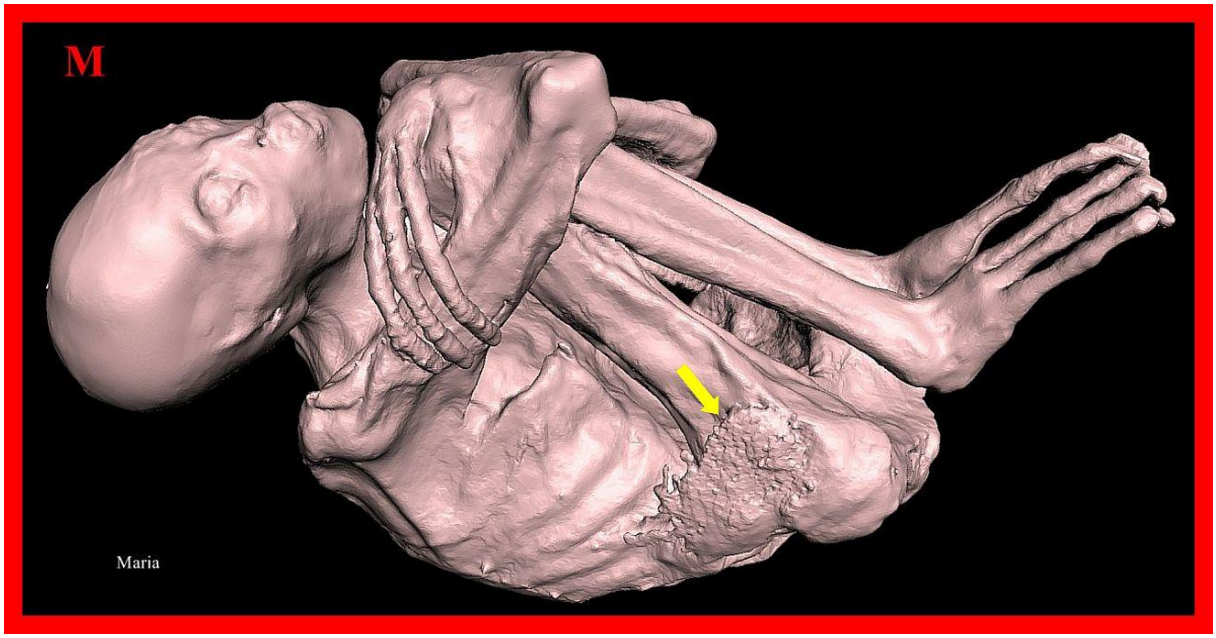

Figure 3: 3D CT of '***Maria***' showing the long tridactyl fingers and toes. Note how the long fingers naturally wrap around the arm. The skin surface is well seen despite having diatomaceous earth covering. However large conglomerate of external materials can be visible *(yellow arrow)*.

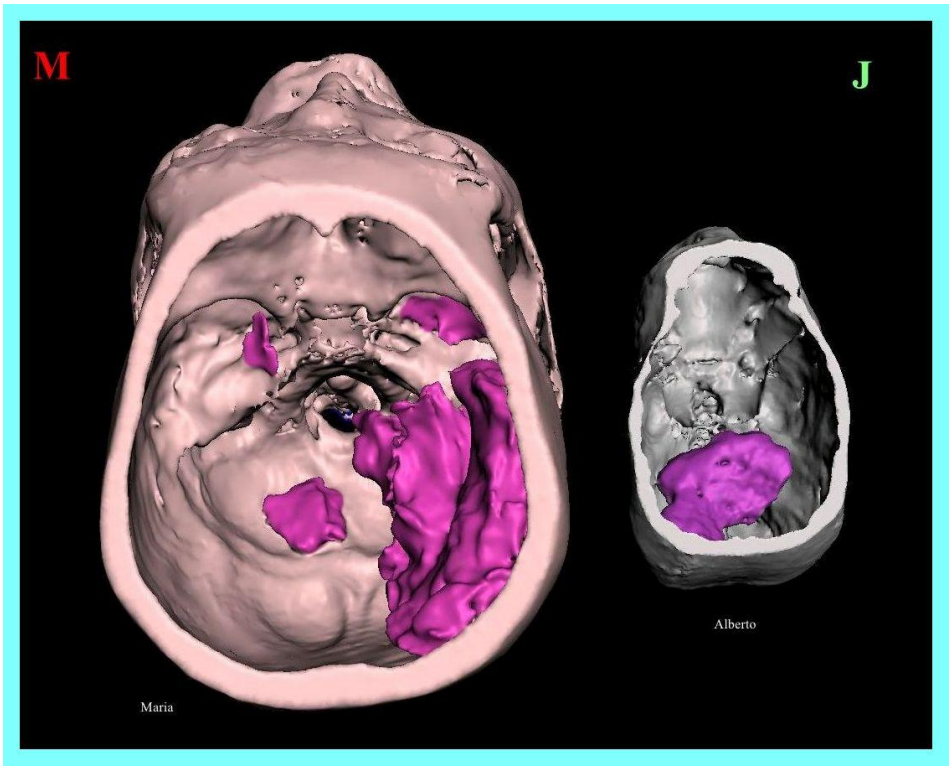

Figure 4: Comparative 3D CT of exposed skull of '***Maria***' *(left image)* and '***Alberto***' *(right image)* showing presence of remnant brain tissues *(coloured lilac)* within the skull.

Figure 5: 3D CT showing front view *(upper image)* and back view *(lower image)* of all metallic implants found in '***Maria***' *(total=1)*, '***Montserrat***' *(total=10)* and '***Sebastian***' *(total=3)*. Note the tool marks on the implants.

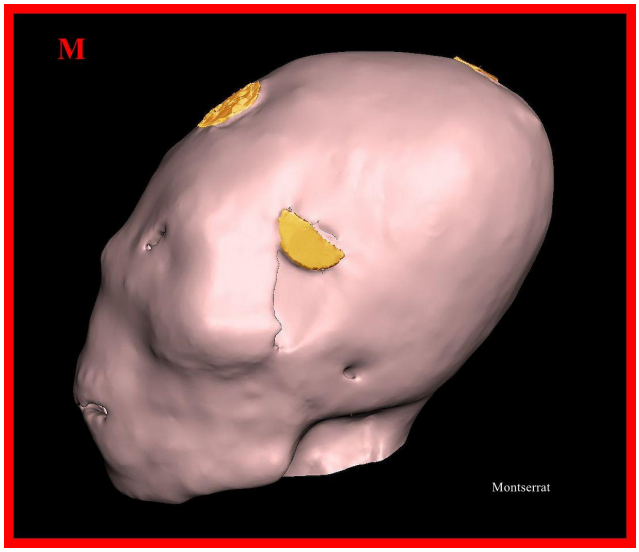

Figure 6: Side view of 3D CT of head of '***Montserrat***' showing metallic implants strategically placed over forehead, vertex and bilateral temporal regions. Note the elongated skull, sloping face and orbits and absence of external pinna.

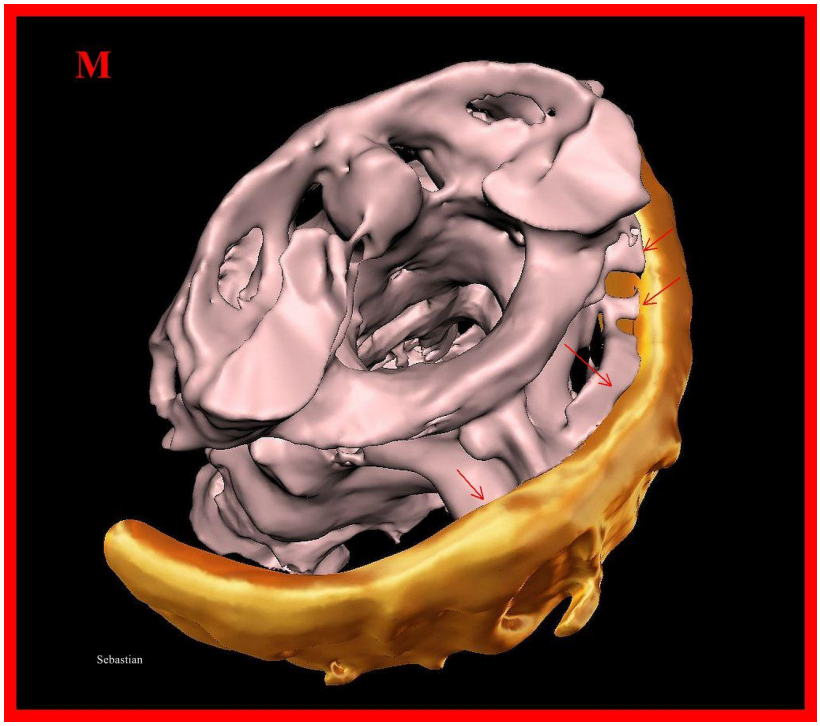

Figure 7: 3D CT of '***Sebastian***' showing dissected view of upper cervical spine and collar-like metallic implant in the back of neck. Note evidence of bone growth that fused with the metallic implant *(red arrows)*. The odontoid process, atlas, axis and spinal canal are well shown.

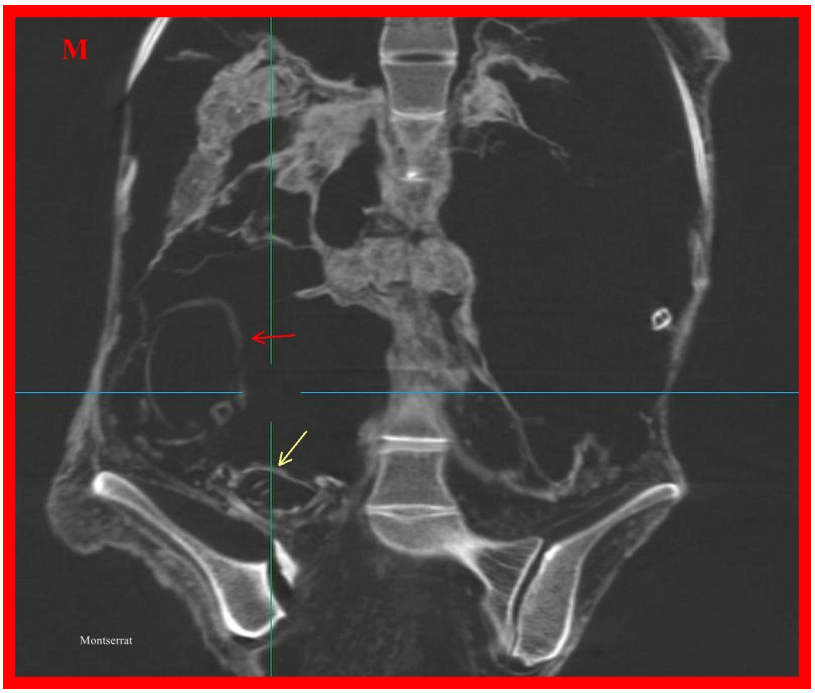

Figure 8: Coronal 2D CT scan showing '***Montserrat***' with single well-formed foetus '***Rafael***' in right side of her abdomen. Note overlapping cranial bones *(red arrow)* and partially collapsed thorax *(yellow arrow)* in '***Rafael***'.

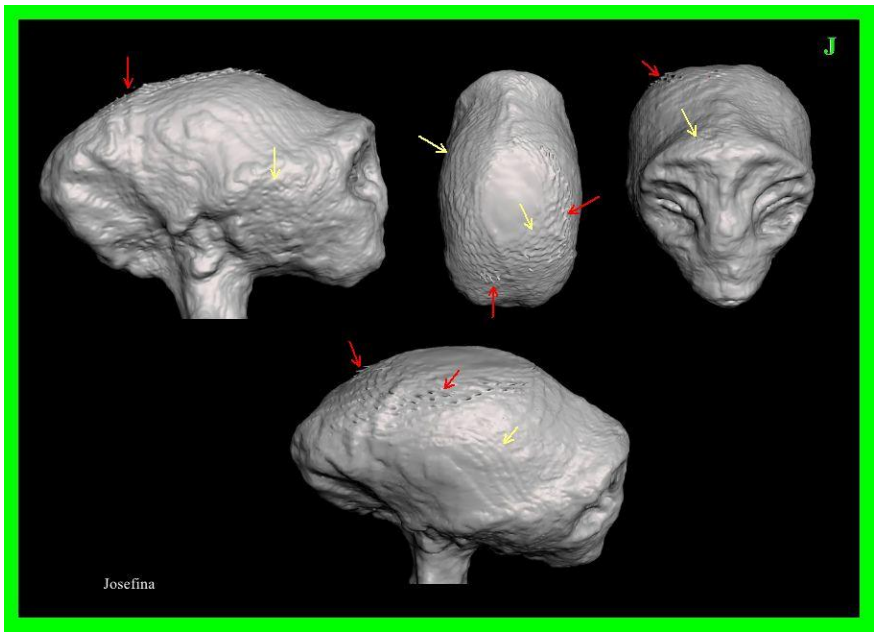

Figure 9: 3D CT with computer enhancement to improve resolution showing bristle-like hairs *(red arrows)* and reptilian skin texture *(yellow arrows)* in head of '***Josefina***'.

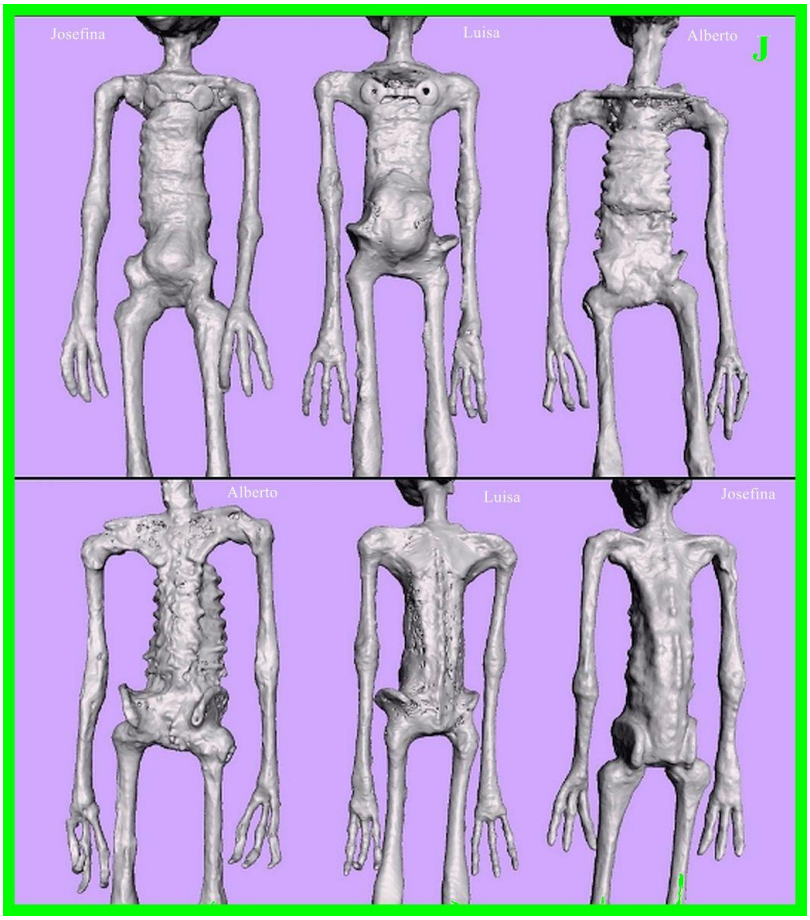

Figure 10: 3D CT showing front *(top row)* and back *(bottom row)* of the J-type tridactyls. Note the tight wrapping of skin that is most pronounced in '***Alberto***' and least so in '***Luisa***'. The pelvic bones also showed striking variations.

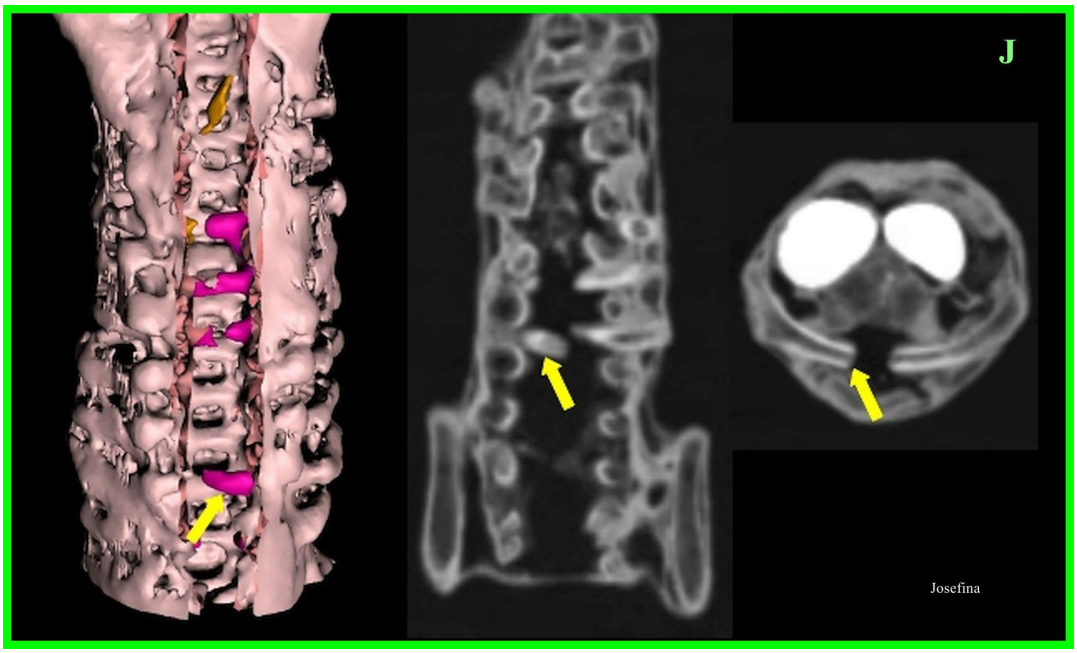

Figure 11: Axial *(right image)* and coronal *(middle image)* 2D CT scans of the spine of '***Josefina***' showing broken ribs *(yellow arrows)* penetrating into spinal canal through the intervertebral foramina. 3D CT *(left image)* digitally removing the dorsal part of the spine to expose the spinal canal showing the protruding ribs *(coloured lilac)*.

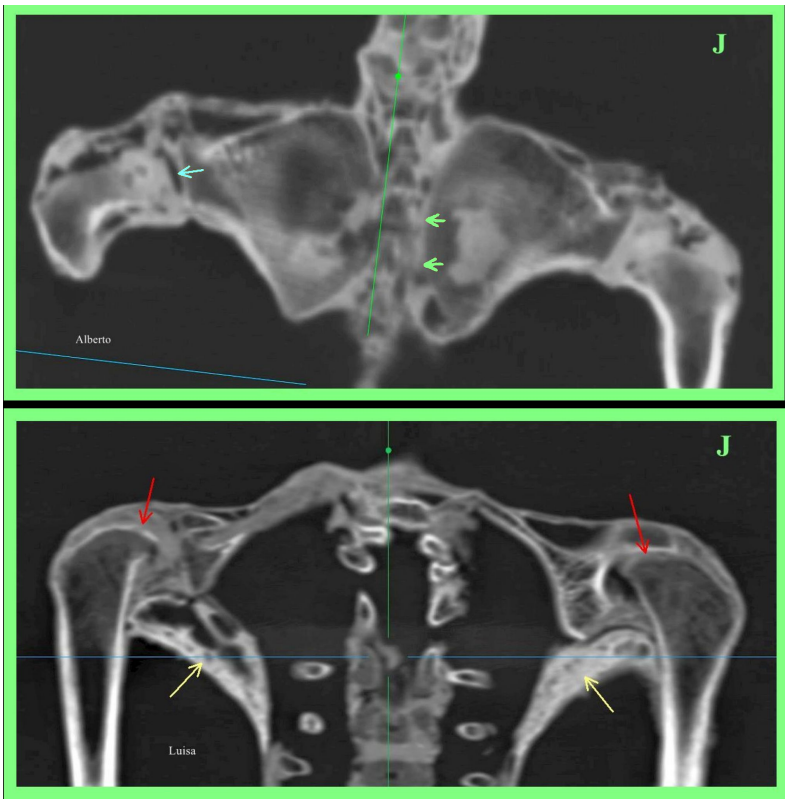

Figure 12: Coronal 2D CT scan showing shoulder joint in '***Alberto***' *(upper image)*. Note the shoulder joint space *(blue arrow)*, the scapulae forming an almost straight plane with fusion of their medial edges to the thoracic spine *(green arrows)*. Coronal 2D CT *(lower image)* of shoulders of '***Luisa***' showing upward subluxation of humeral heads *(red arrows)* and presence of extensive haematoma in bilateral arm pits *(yellow arrows)*.

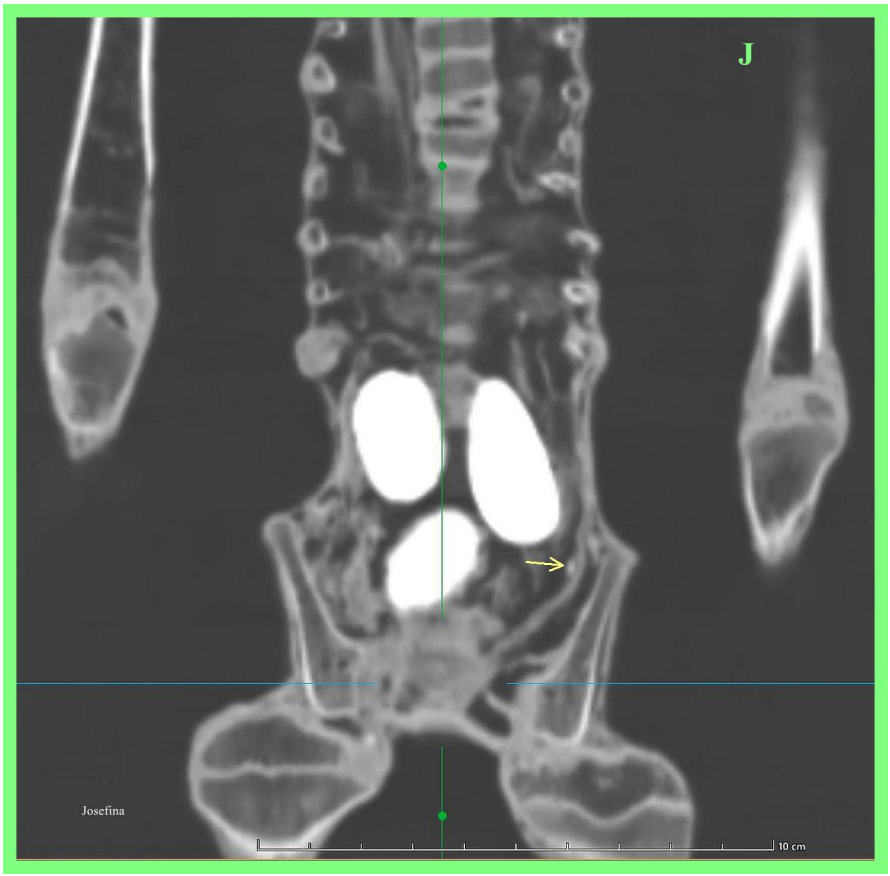

Figure 13: 2D coronal CT scan of '***Josefina***' showing 3 large eggs in abdomen. The tiny 4th egg can be found on the left side of abdomen *(yellow arrow)* and a fifth tiny egg can be found inferiorly and anteriorly *(see Figure 44)*. Note the extremely unusual finding of high density of the egg content. The CT value is even higher than bone and approaches that of the metal implant.

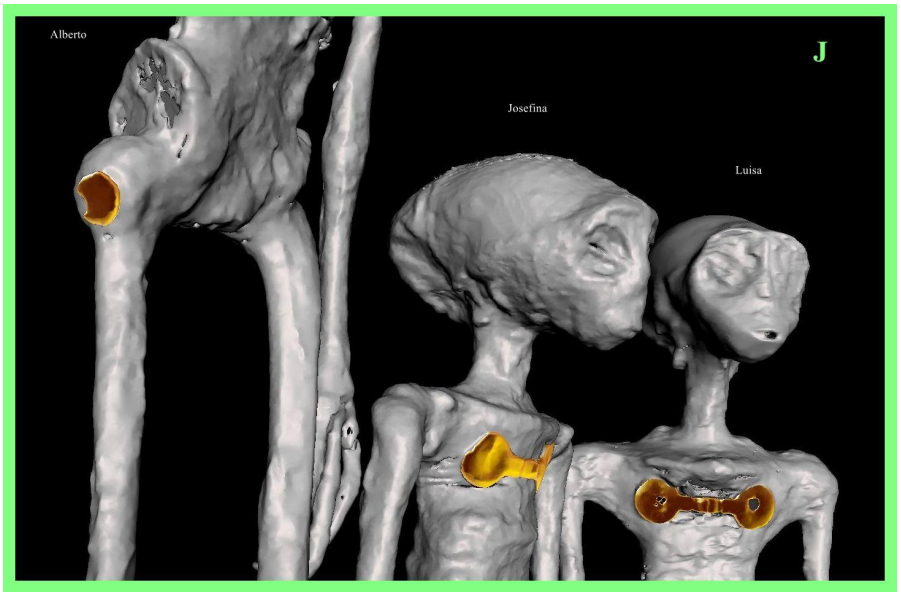

Figure 14: 3D CT showing right hip implant in '***Alberto***' *(left)* and dumbbell-shaped implants in '***Josefina***' *(middle)* and '***Luisa***' *(right)* below their furcula.

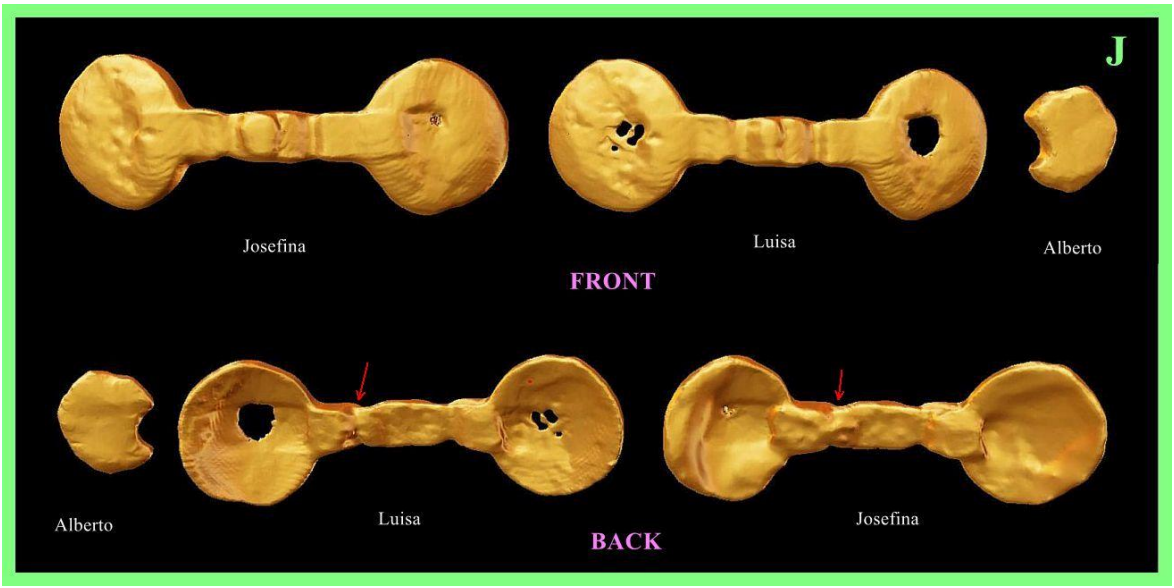

Figure 15: 3D CT showing front view *(upper row)* and back view *(lower row)* of metallic implants found in J-type tridactyls. Note the exquisite and similar design with tool marks on the dumbbell-shaped chest implants in '***Josefina***' and '***Luisa***'. There is suspicion of locking mechanism in the central bars *(red arrows)*.

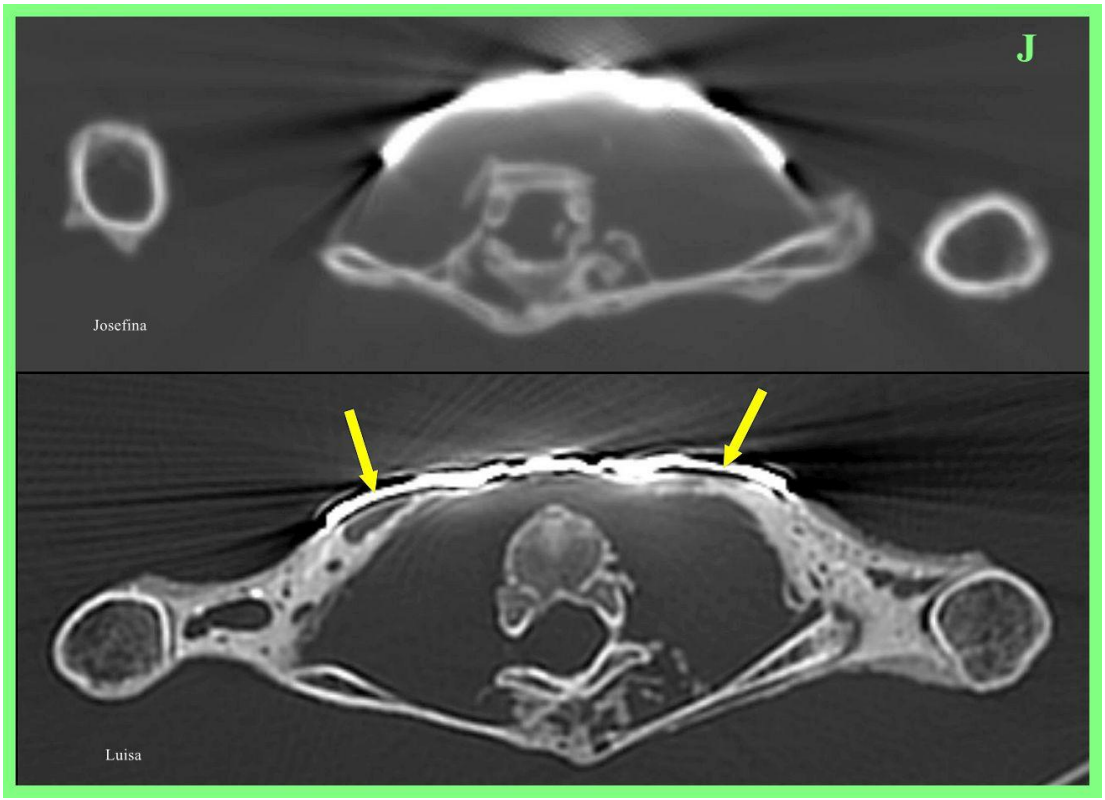

Figure 16: 2D axial CT scans showing metallic chest implants in '***Josefina***' *(upper image)* and '***Luisa***' *(lower image)*. Note the metal causing streaking 'beam hardening' CT artefacts in both implants and the composite nature of the implant with dense core *(yellow arrows)* in '***Luisa***'.

SECTION 3: HEAD AND NECK

M-type tridactyls:

- The 'M' type tridactyls show varying degree of elongated skull with the vertex shifted posterior and superiorly. *(Figures 1,3,6,17,19)*

- All lack coronal and sagittal sutures externally although the fused suture could still be identified on cross section of the bones. *(Figure 19)*

- Enlarged sloping orbits are noted. Elongated eye slits are tilted upwards and laterally. Orbital contents can be identified. *(Figures 17,19,25)*

- Essentially the head of M-type tridactyls resembles human skull in the presence of various distinct compartments including cranium, orbits, facial bones, petrous, paranasal sinuses and mandible. However, there are distinct differences as compared with human. *(Figures 21,22,25,27)*

- Facial bones and sinuses are relatively small compared with human.

- Nose including 2 nostrils shows variability in size, shape and location and are non-human-like in '***Sebastian***'. *(Figure 17)* Internally, the inferior nasal passage appears to be relatively enlarged.

- All show lack of external pinnae. *(Figures 1,3,6,17,19)* Petrous bones, ear canal, middle and inner ear structures however resemble human configuration. *(Figure 27)*

- Foramen magnum, axis and odontoid resemble human configuration. *(Figures 7,23)*

- The lower jaw is protruding with obtuse angles in mandible. Children and adult sets of teeth are similar to human. *(Figure 27)*

- Cervical spine is similar to human.

SECTION 3: HEAD AND NECK (contd.)

J-type tridactyls:

- The bony anatomy is entirely different from human nor M-type tridactyls.

- The skull is large relative to the body. The skull is represented by a single hollow bony structure without differentiation into different compartments such as cranium, paranasal sinuses, oral cavity or mandible. The sizes, shape, facial and bony features show individual variations. *(Figures 20,21)*

- Brain remnants can be found in the skull of '***Josefina***' and '***Alberto***'. *(Figures 4,21,59)*

- The skull is scaphoid in shape and elongated antero-posteriorly. It is convex superiorly and laterally. Subtle V-shaped bone ridges converging anteriorly can be found on the superior aspect of the skulls externally. *(Figure 20)*

- Fronto-parietal suture and occipital suture can be identified. The convex part of the skull is smooth and devoid of sagittal suture. *(Figure 20)*

- Posteriorly, the occipital part of skull bone shows an inverted triangular shape with rough surface and variable bone thinning bearing large bony sinuses. There is midline bony ridge inferiorly extending towards the foramen magnum, again containing bony sinuses. Distinct large bony concavities anterior to occipital region bilaterally can represent insertion sites for neck muscles. *(Figure 18)*

- Anteriorly, there is prominent supra-orbital ridge delineating the facial bones. A T-shaped bony ridge is formed when the supraorbital ridge meets the midline bony ridge between the orbits extending to the vestigial nose. A shallow bony depression could be found behind the supra-orbital ridge. *(Figures 18,20)*

- On the inside, the skull shows distinct convolution markings corresponding to the brain occupying the bulging part of the skull. Anteriorly it is bordered by a wide groove presumably representing major venous sinus deep to the depression behind the supraorbital ridge. *(Figure 22)*

SECTION 3: HEAD AND NECK (contd.)

J-type tridactyls (contd.)

- Anterior and inferior to the brain markings are found 2 distinct otic capsules on the inner surface of the skull showing high density (CT value similar to metal implant and greater than limb or skull bones). *(Figure 27)* Large internal auditory meati can be found in the optic capsule. *(Figures 27,31)* Internal structures are noted in the otic capsule that could represent vestibule and semicircular canals. *(Figure 28)* However the ear structures are completely different from M-type tridactyls or human. Notably, in '***Alberto***' the left otic capsule is located at an unusually high location. On the other hand, the right otic capsule is absent and replaced by a thin bony plate. *(Figures 29,30)*

- There are numerous sinus-like spaces in-between the skull bones. Large sinus-like spaces are noted behind the supraorbital ridge, in the face, occipital region and in skull base behind foramen magnum. *(Figures 31,32)*

- The basal part of the skull is irregular in shaped with focal bulges and depressions externally and featuring irregular bone thinning. The neck joins the head in its mid third (unlike M-type namely in the posterior third). *(Figures 30,32)* Two prominent elongated narrow mastoid-like bony projections containing air cells internally are noted in the base of the skull at both sides of the neck. *(Figures 18,33)*

- The foramen magnum is roundish (NOT SQUARE) in shape but there is lack of atlas-odontoid arrangement. *(Figure 24)* The first cervical spine is found within the foramen magnum.

- The face shows cordiform-shape with wide forehead and symmetrical bilaterally enlarged orbits, small facial bones tapering to a small chin. The disproportionally large orbits are represented by two oval-shaped slightly concave thin orbital bony plates, each bearing an obliquely orientated gap in its middle tilted upwards and laterally, mirroring the appearance on the skin. There is shallow depth between the skin and the bony orbital plates, quite different from the deep orbits in M-type tridactyls. *(Figures 18,20,22,26)*

- On either side of the face, there are multiple bony depressions with bony thinning covered by thin membrane. The function of these depressions remain speculative ? for respiration, hearing or thermal regulation or thermal detection. *(Figure 33)*

- The nose is rather indistinct. No apparent nostril is visible on the skin. Bony nostrils are variable and not found in '***Josefina***'. *(Figures 18,20,36)*

SECTION 3: HEAD AND NECK (contd.)

J-type tridactyls (contd.)

- The mouth is protruding, small, conical in shape and formed by an upper and a lower oval-shaped bony mouth plate showing hinge joints at their sides with attachment superiorly and inferiorly to the rest of the skull. No teeth is found. Posteriorly, the inferior mouth plate leads to a depression or hole through the bony compartment into the inferior part of the chin. A flat hollow palate-like bone is found behind the opening that may contain an irregular sinus. Below the bony plate, a pharynx-like structure is found on the underside of the chin. It then divides into a tubular airway anteriorly and a wider irregular food channel posteriorly. *(Figures 18,31,32)*

- There is very thick skin covering in the neck that may serve as an exoskeleton. The length of the neck varies significantly with longest neck found in '*Alberto*'. *(Figure 2)*

- A prominent venous structure is found in right side of neck extending to a plexus at skull base bilaterally. *(Figure 34)*

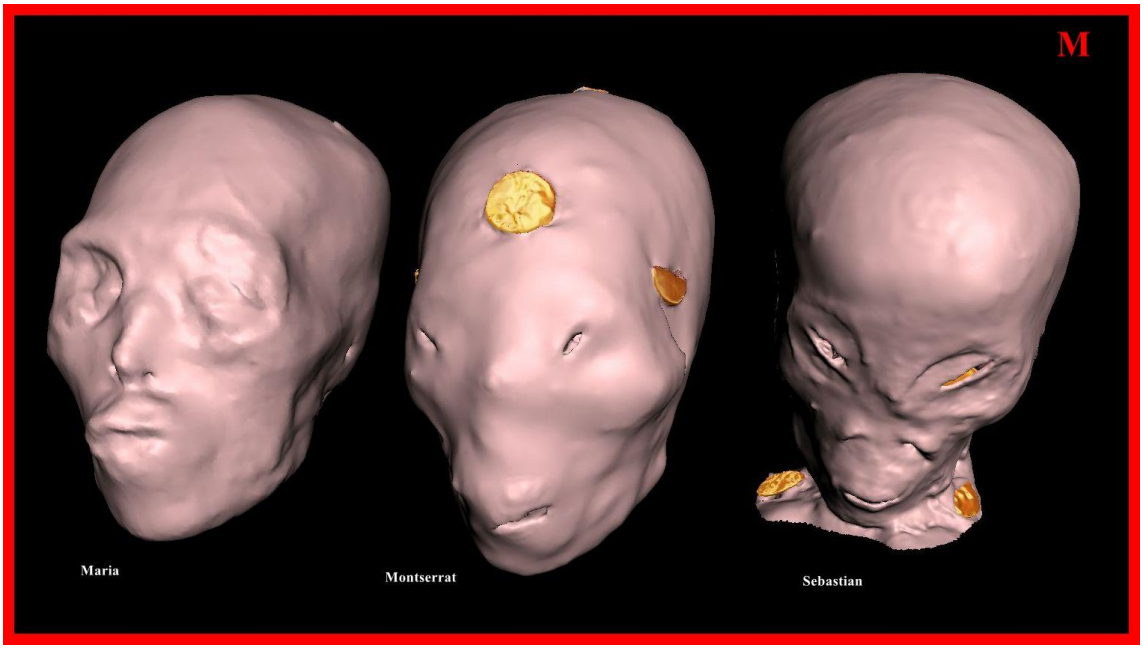

Figure 17: 3D CT showing wide variations in facial features in the M-type tridactyls. Note the lack of external pinnae, slanting eyelids and variations in the nose and nostrils.

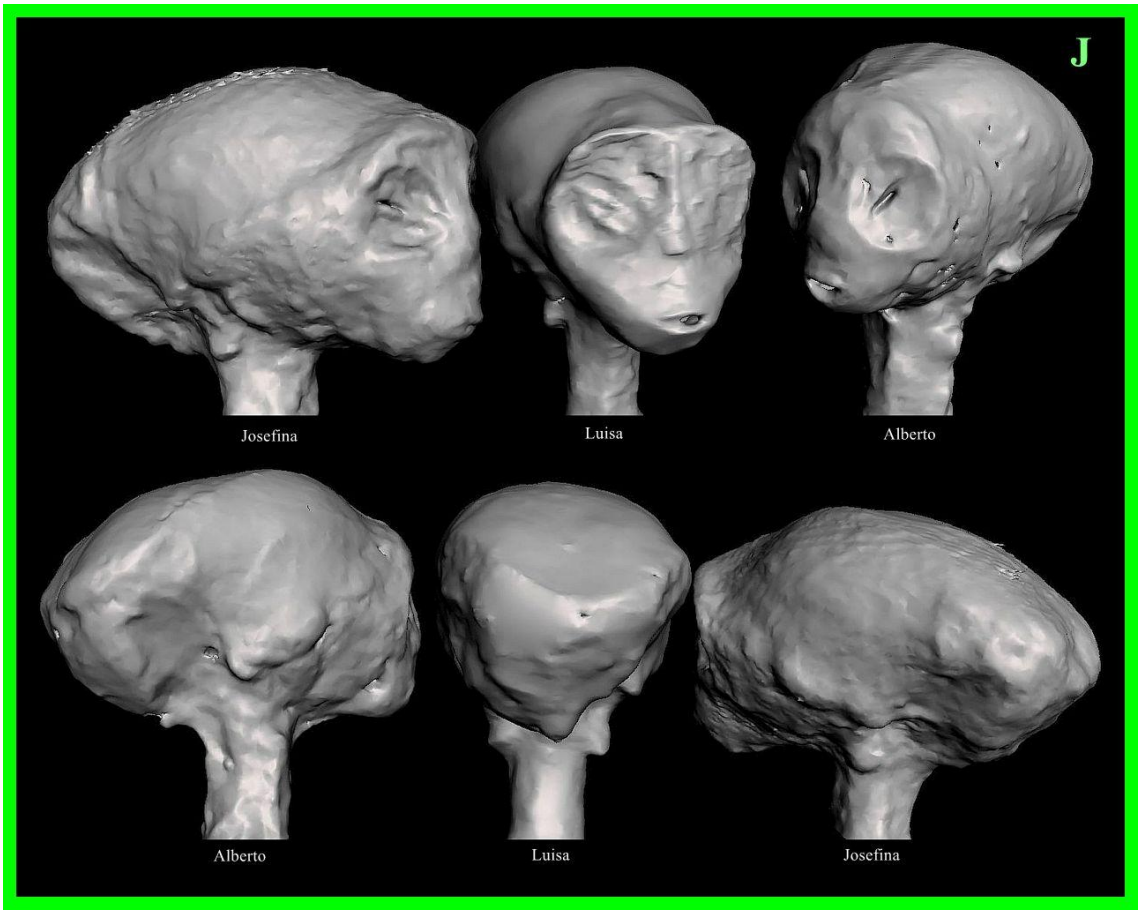

Figure 18: 3D CT showing heads of J-type tridactyls. All with similar structures showing cordiform-shaped face, enlarged eyes sockets, enlarged slanting eye slits, small conical shaped mouth, triangular shaped occiput, bilateral narrow mastoid-like bony processes besides neck and absence of external ear. However noted individual variations in the supra-orbital ridges and facial features.

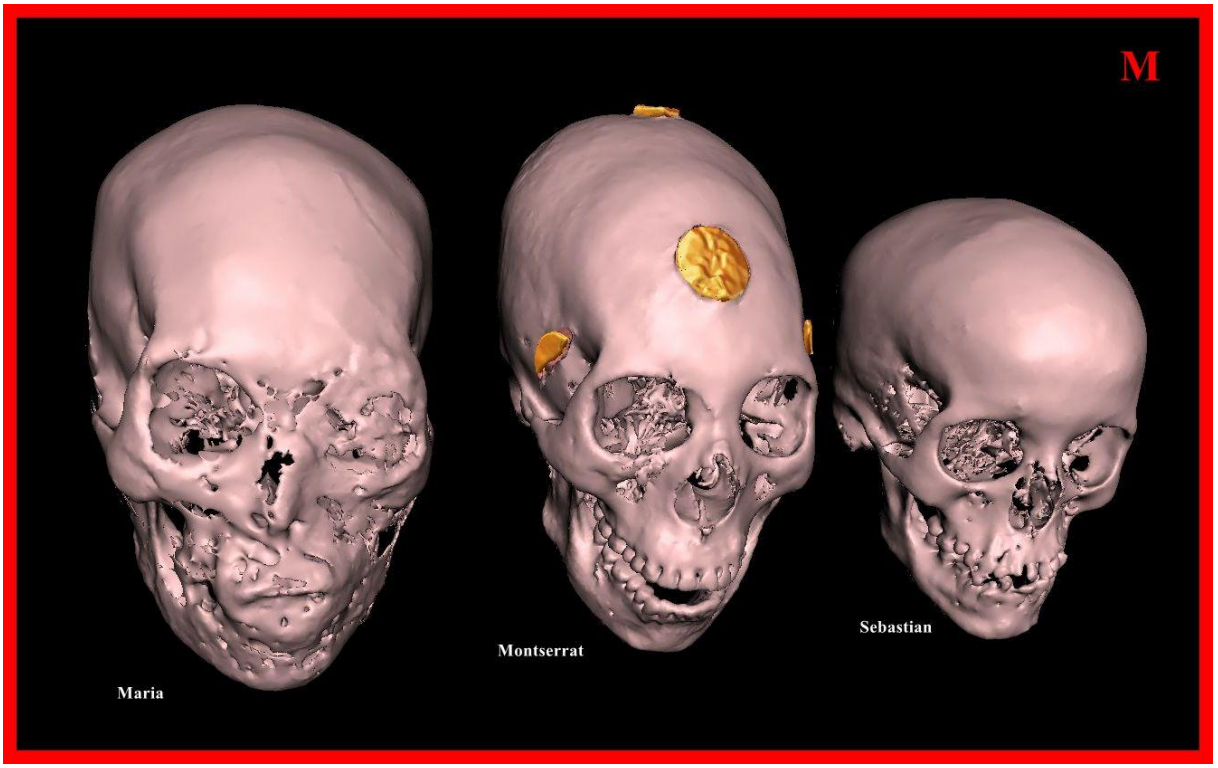

Figure 19: 3D CT showing skulls of the M-type tridactyls. Note the elongated skulls, enlarged orbits and presence of teeth. Metallic implants on the head of '***Montserrat***' are also shown.

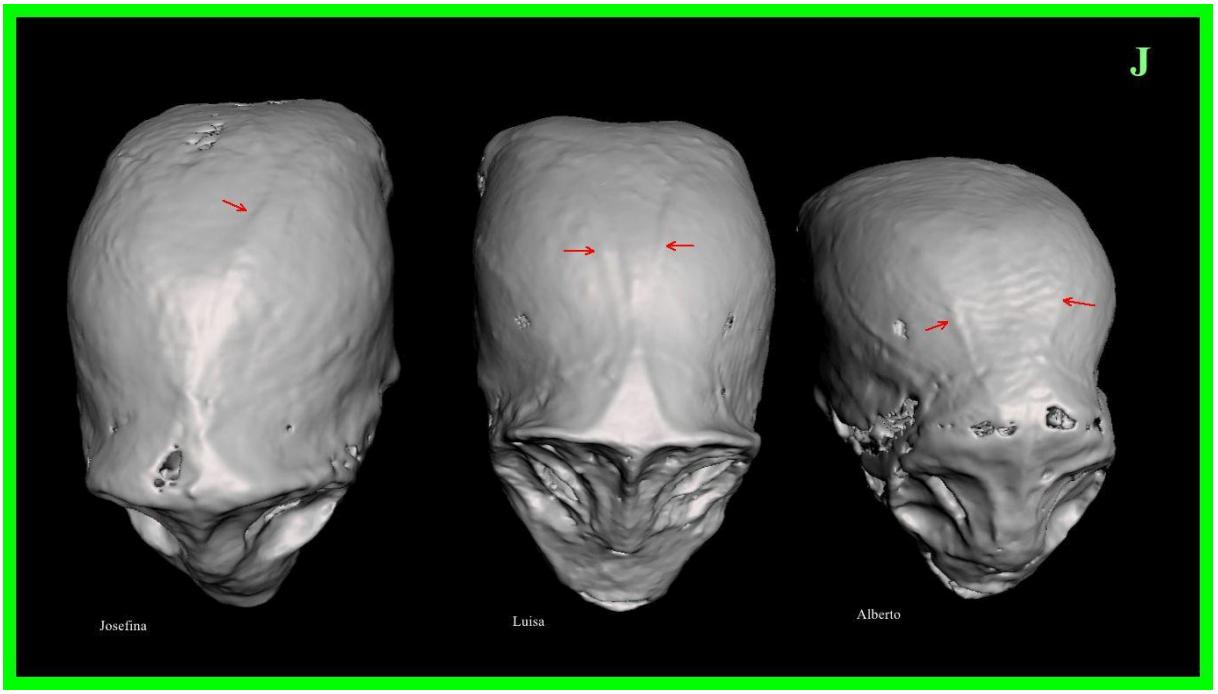

Figure 20: 3D CT showing the skulls of J-type tridactyls. Note the scaphoid shaped skull, shallow enlarged orbital plates with slanting slits, V-shaped ridges *(red arrows)* on the top part of skull. Noted the variations in supra-orbital ridge.

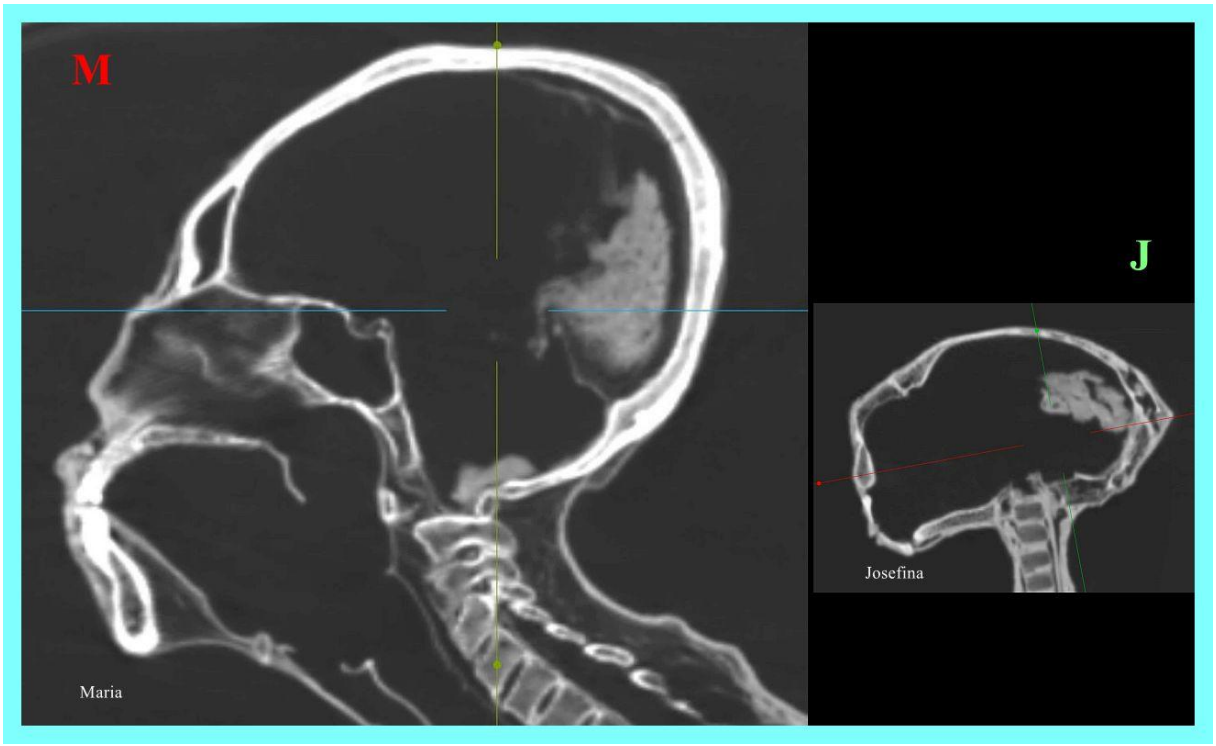

Figure 21: 2D sagittal CT scans of skull comparing '***Maria***' *(left)* with '***Josefina***' *(right)*. Note the different compartments within the skull in the M-type tridactyl as compared with the single compartment in the skull of J-type tridactyl. Residual brain tissue can be seen in both.

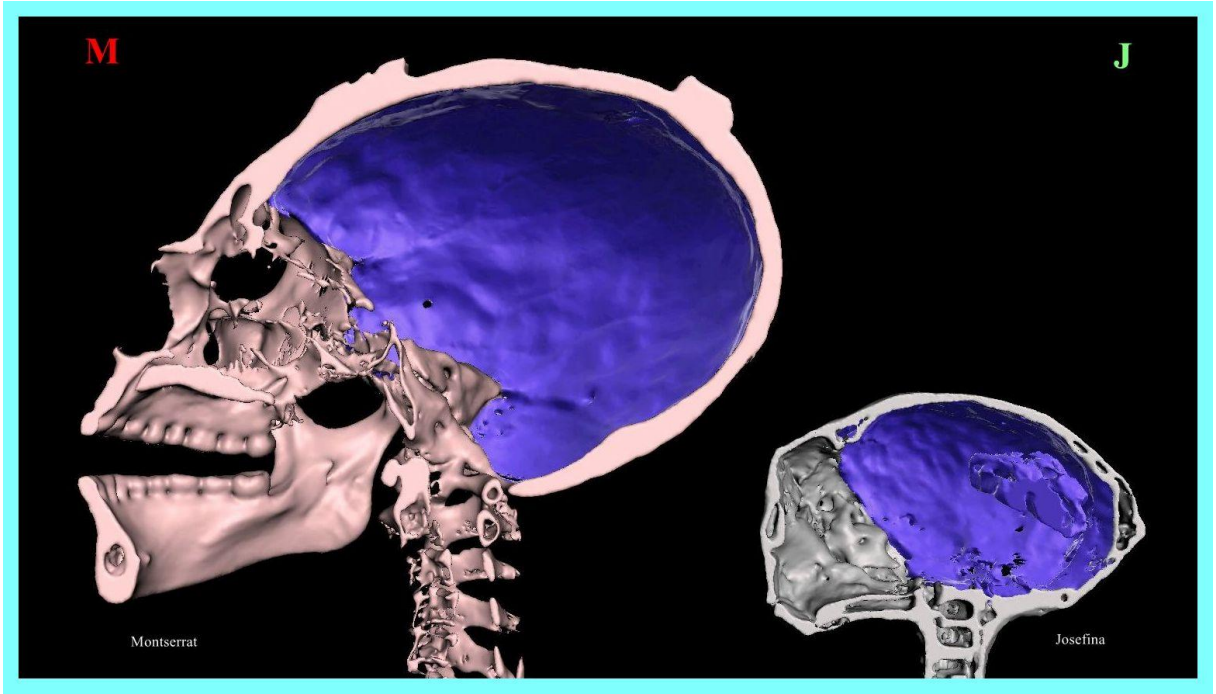

Figure 22: 3D CT sectioned skull comparing '***Montserrat***' *(left)* with '***Josefina***' *(right)*. The convolution markings on the inner surface of the skull provide clue to the location of the brain *(in purple)*.

Figure 23: 3D CT showing the oval shaped foramen magnum of '***Montserrat***' as viewed from above. Note the peg-like odontoid process and the arch of the atlas posteriorly.

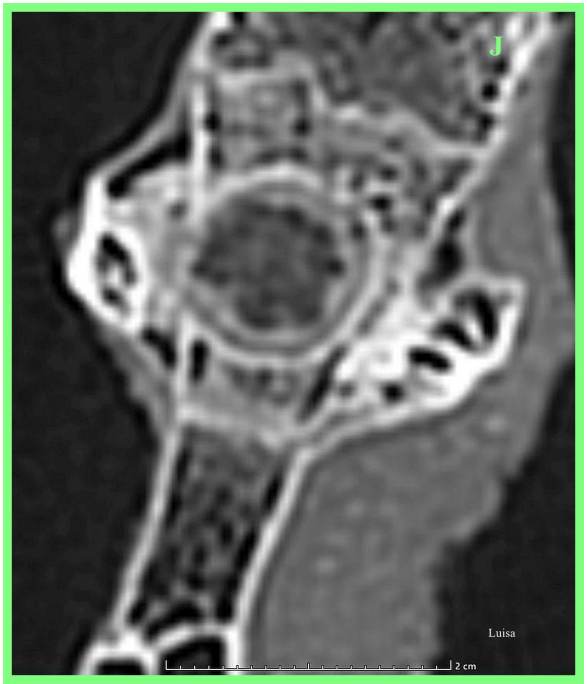

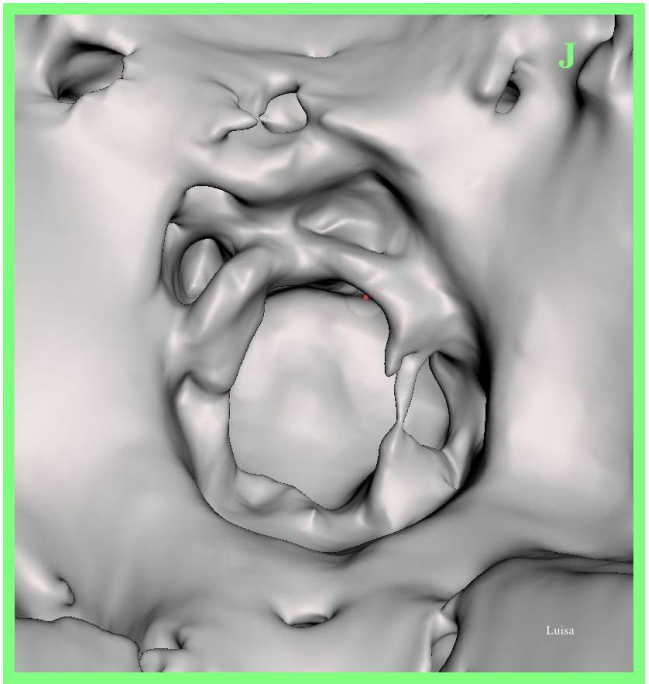

Figure 24: Foramen magnum of '***Luisa***'. 2D axial CT scan *(left image)* and 3D CT as viewed from above inside the skull *(right image)*. CT scan confirmed that the foramen magnum is roundish and refute any claim that it is square in shape.

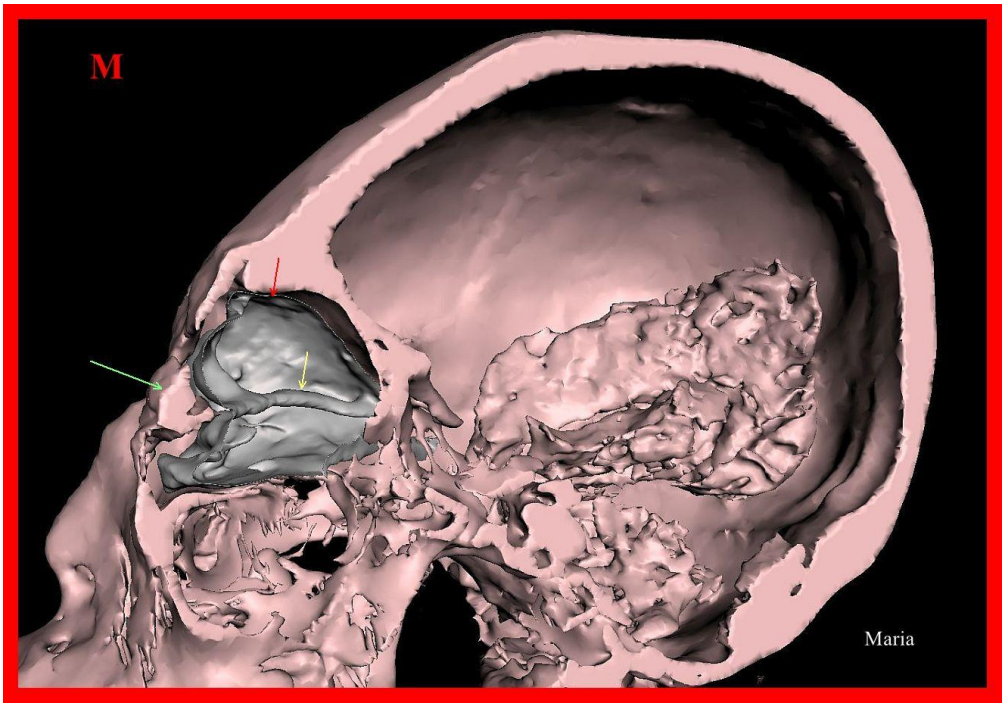

Figure 25: Sectioned 3D CT of skull of '***Maria***' showing sloping face, left orbit and forehead. The enlarged distorted orbit contains a large remnant eye structure *(red arrow)* with central chord-like hyaloid canal *(yellow arrow)*. The left eyelids *(green arrow)* are swollen, presumably due to trauma. Residual brain tissue can also be seen inside cranium.

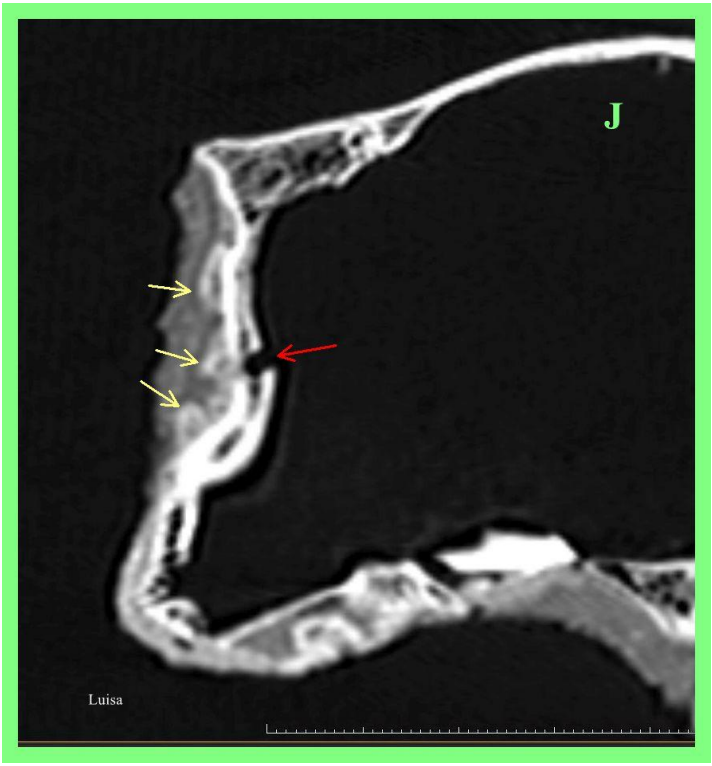

Figure 26: 2D sagittal CT scan of '***Luisa***' showing slit-like opening in the left orbital plate *(red arrow)*. The orbital bone shows shallow concavity. Unilateral soft tissue swelling in left orbit and prominent residual orbital content *(yellow arrow)* are probably result of trauma.

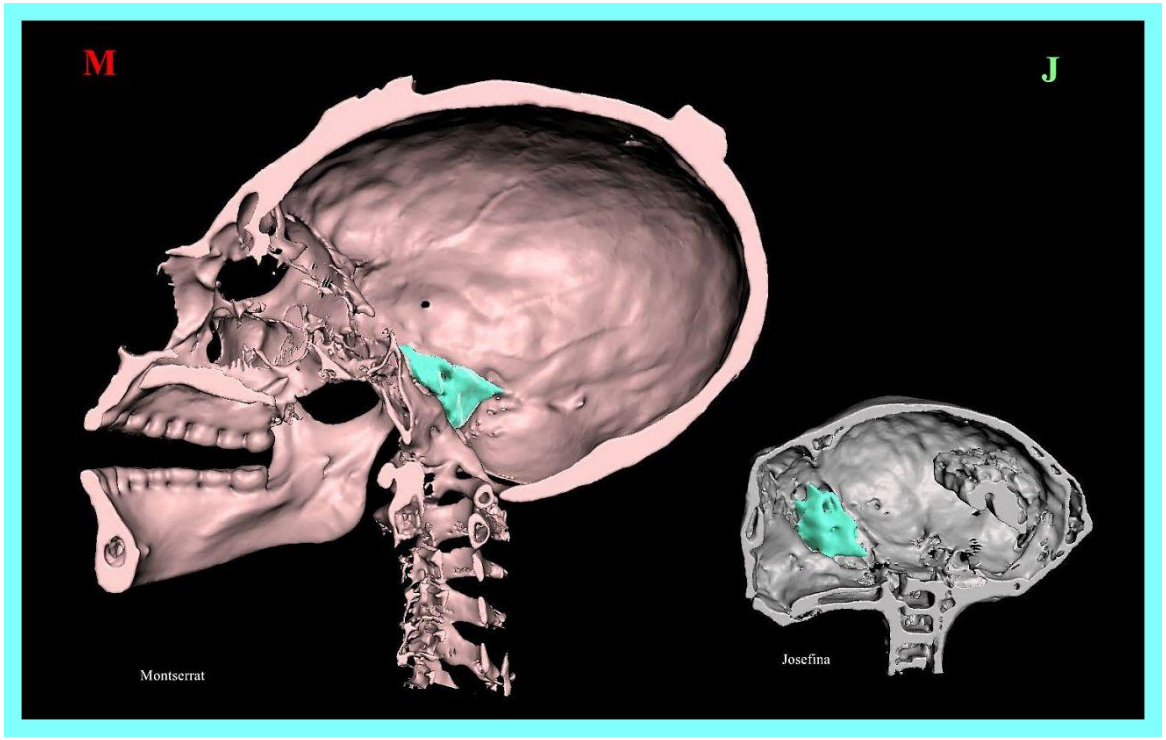

Figure 27: 3D CT showing comparative views of right halves of the skulls and necks of M-type and J-type tridactyls. Similar to human, the organ of hearing in M-type tridactyl is located inside the petrous bone on either side of foramen magnum. In the J-type tridactyl, the otic capsule shows entirely different morphology and is located in the anterior 1/3 of the skull in a more forward location anterior to the foramen magnum.

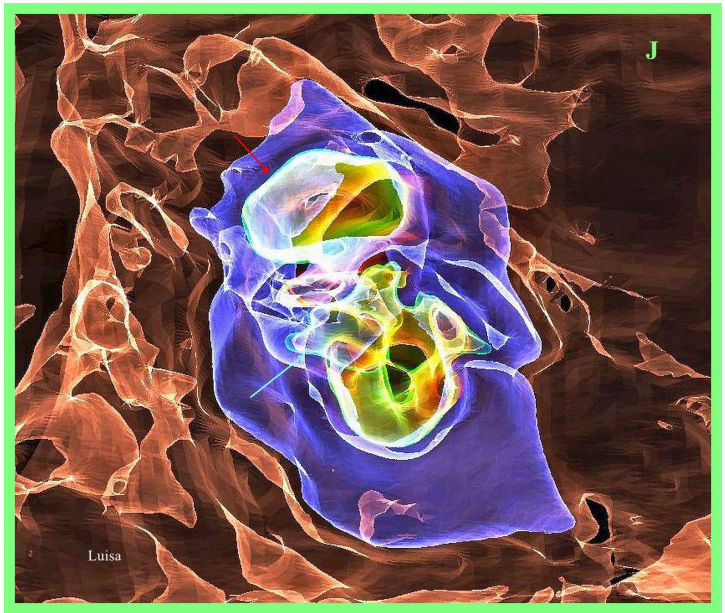

Figure 28: 3D CT in semi-transparency showing otic capsule of '***Luisa***'. Inside the otic capsule, the internal auditory meatus *(red arrow)* leads to a an oval shaped structure above and an irregular structure below *(blue arrow)* presumably bearing semi-circular canals. *(Note: left side of image is facing anteriorly).*

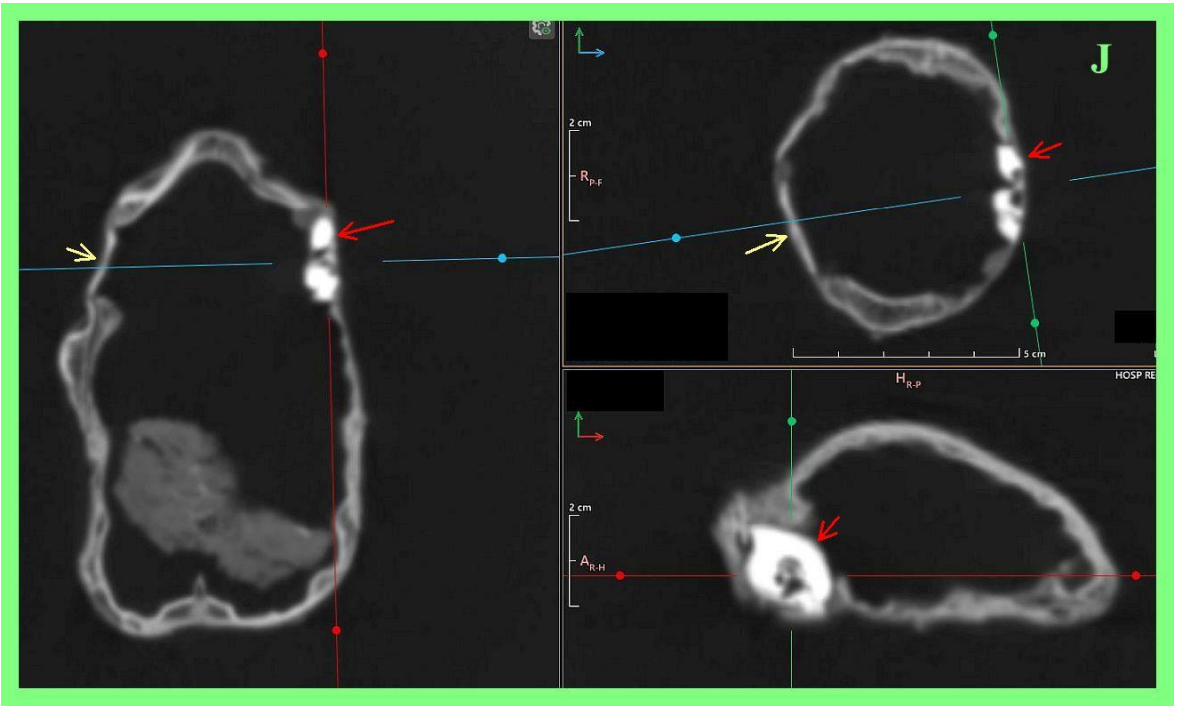

Figure 29: 2D CT scans with multi-planar reconstruction showing the hyper-dense left otic capsule *(red arrow)* in '***Alberto***'. The right otic capsule is absent and is replaced by a flat piece of bone. *(yellow arrow)*. This appearance could have occurred if the right otic capsule had been surgically resected and the defect being fitted with bone graft.

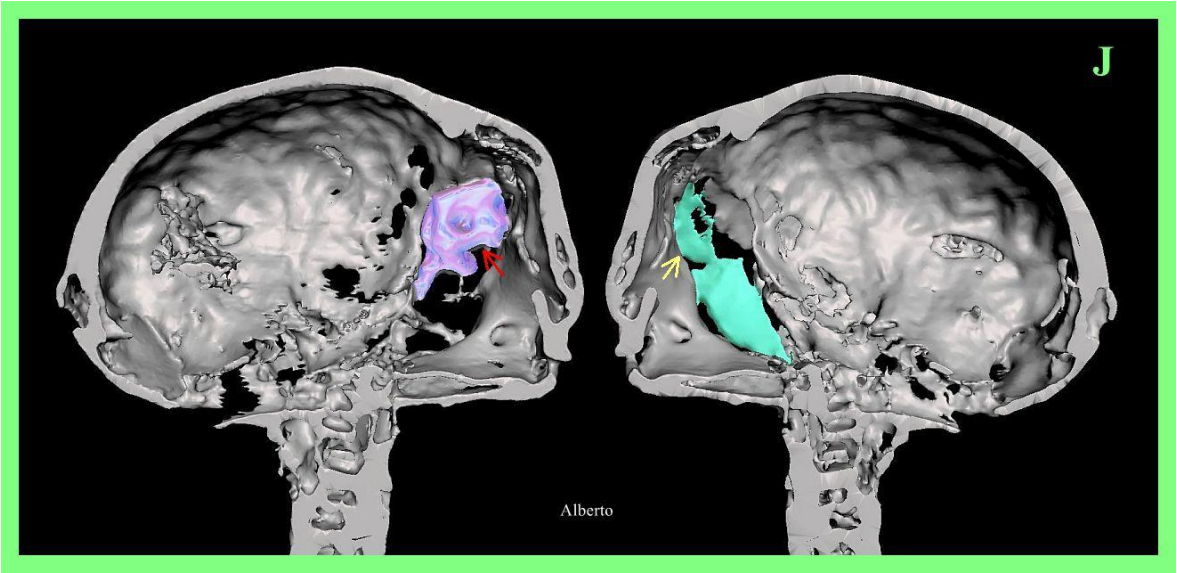

Figure 30: 3D CT scan of the left *(left)* and right *(right)* halves of the skull of '***Alberto***'. The left otic capsule *(red arrow)* is intact but is in a higher location as compared with '***Josefina***' and '***Luisa***'. A presumed bone graft is in place in lieu of the absent right otic capsule *(yellow arrow)*.

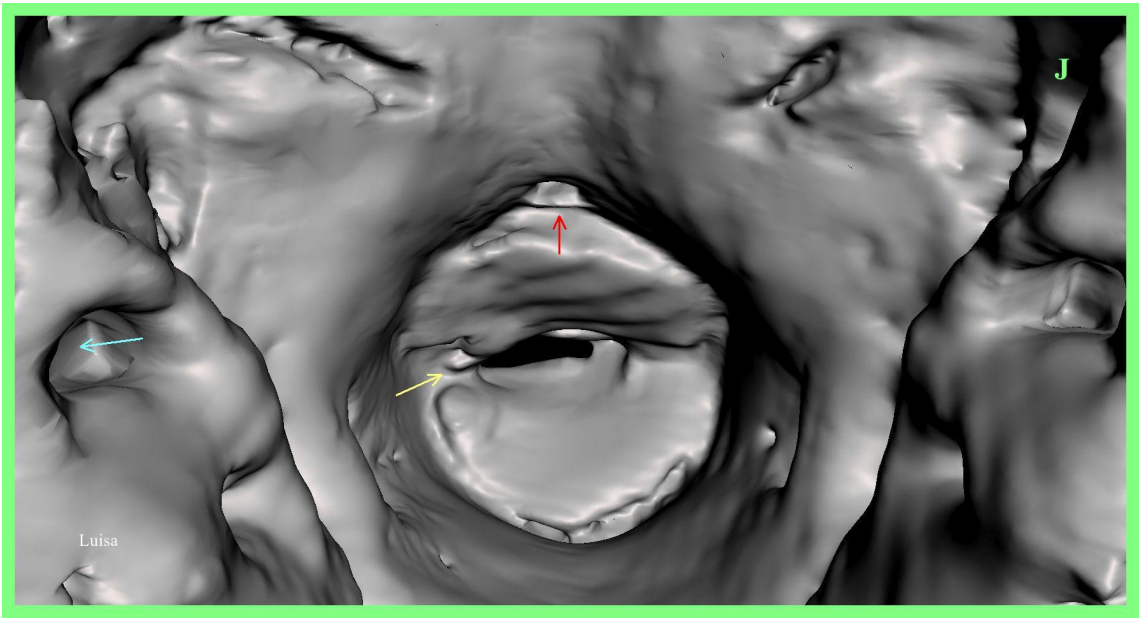

Figure 31: 3D CT of '***Luisa***' showing virtual reality view from inside the mouth looking forward. The upper and lower mouth plates can be seen in the centre with hinge joint on its side *(yellow arrow)*. The opening to the frontal sinus is seen in midline above the upper mouth plate *(red arrow)*. On either side, the internal auditory meatus of the otic capsule can be seen *(blue arrow)*.

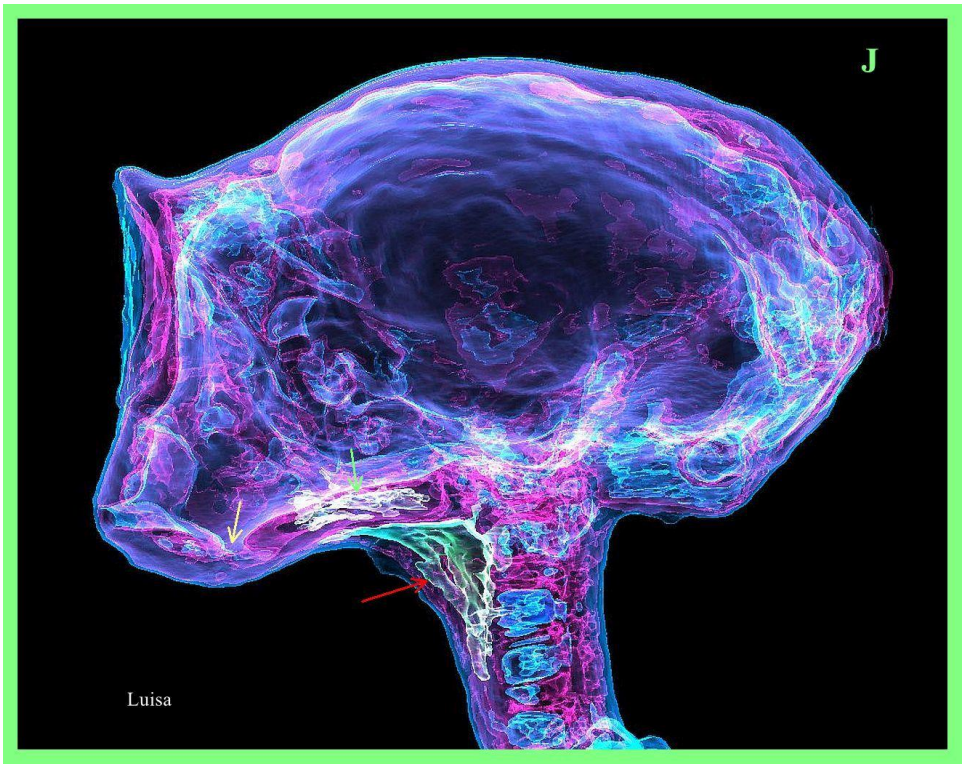

Figure 32: 3D CT of '***Luisa***' in semi-transparency showing the gap behind the lower mouth plate *(yellow arrow)*. An irregular sinus space *(green arrow)* is seen in the hollow of the flat bony floor of the mouth. Below the bony plate, the pharynx leading to the upper airway in front of the upper neck *(red arrow)* can be found. Note the numerous sinus spaces within the skull in occipital region posteriorly and inferiorly as well as behind the supraorbital ridge.

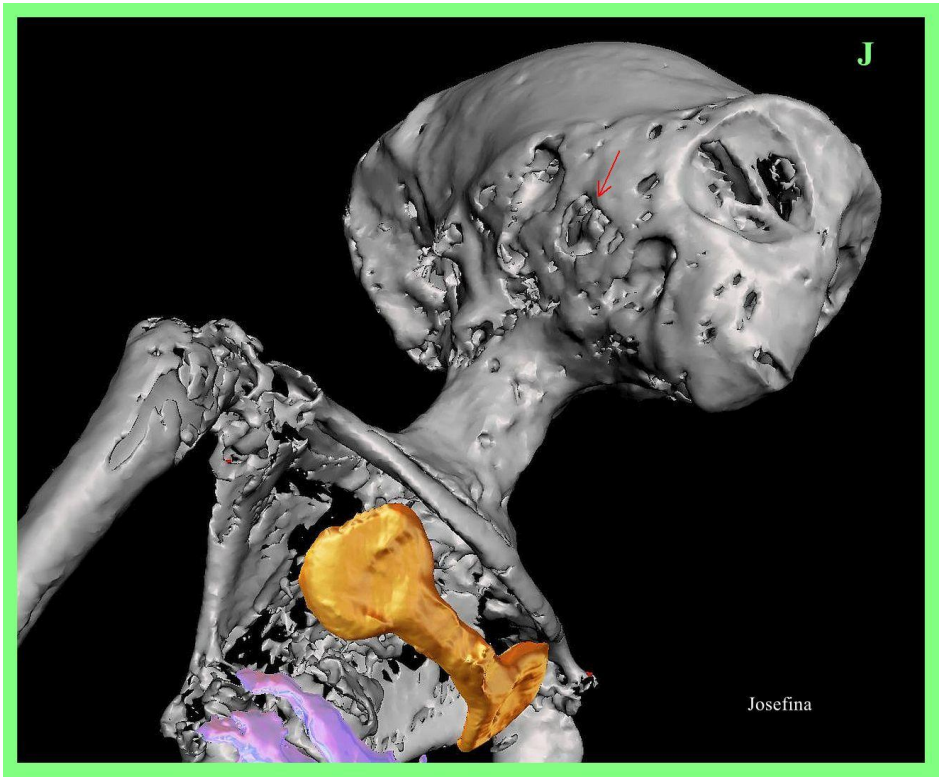

Figure 33: 3D CT of '***Josefina***' showing areas of bony thinning and pit-like depressions in the face. Location of right otic capsule is marked *(red arrow)*.

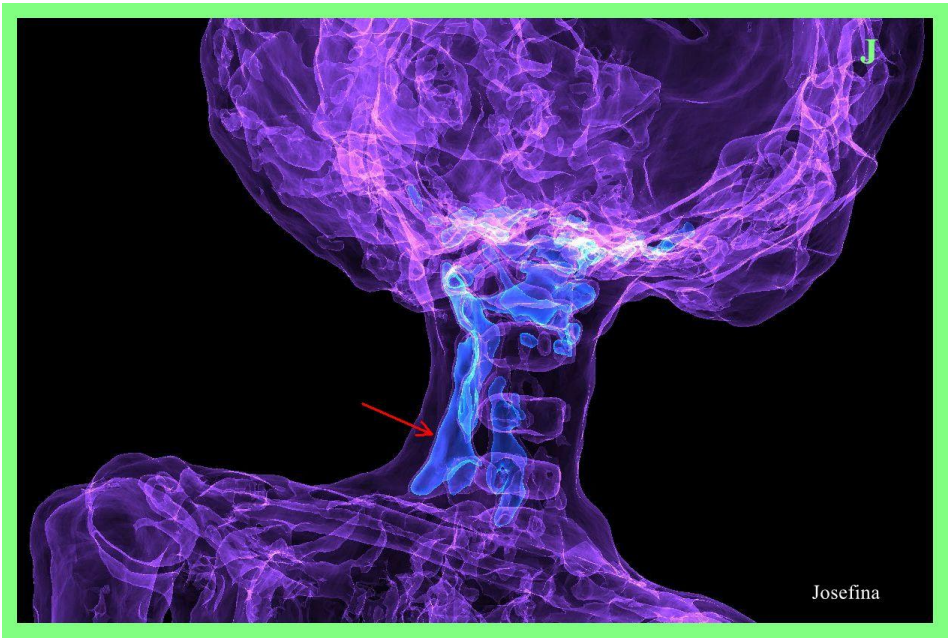

Figure 34: oblique view of 3D CT of '***Josefina***' in semi-transparency showing prominent veins *(red arrow)* in right side of neck communicating with a plexus below the skull.

SECTION 5: THORACIC CAGE

M-type tridactyls:

- The configuration of the thoracic cage is similar to human with ribs, costal cartilages, manubrium and sternum.

- '***Maria***' and '***Montserrat***' show depressed sternum. Exuberant, robust and deformed costal cartilages in the depressed anterior chest wall are found in '***Sebastian***' unlike normal human anatomy. *(Figure 35)*

- The internal anatomy is basically similar to human. Bronchi, pulmonary artery, aorta and left sided 4-chamber heart can be identified.

- Breast with nipple are noted in '***Maria***' and '***Monserrat***'.

J-type tridactyls:

- The structure of the thoracic cage is completely different from human or M-type tridactyls.

- The air-filled lung cavity is butterfly in shape with posterior surface conforming to the shape of the scapulae with the spine in between. Superiorly and posteriorly, it extends above the furcula. Its anterior surface is located between the furcula and the gastralia with thin skin covering anteriorly. *(Figures 36,37,38)* However, differing from the other 2 specimens, the space between the furcula and the upper margin of the gastralia is relatively small in '***Luisa***' so that the lower part of the metal implant is resting on the upper part of the gastralia.

- Sophisticated dumbbell-shaped metallic implants are found below the furcula in '***Josefina***' and '***Luisa***'. The implants are similar in shape but differing in fine details e.g. the implant in '***Luisa***' has a sandwich appearance showing central core of more dense metal. *(Figures 14,15,16,33,36)*

- A rudimentary tubular heart is suspected in the thorax on right side of the spine just above the level of the gastralia. *(Figure 37)*

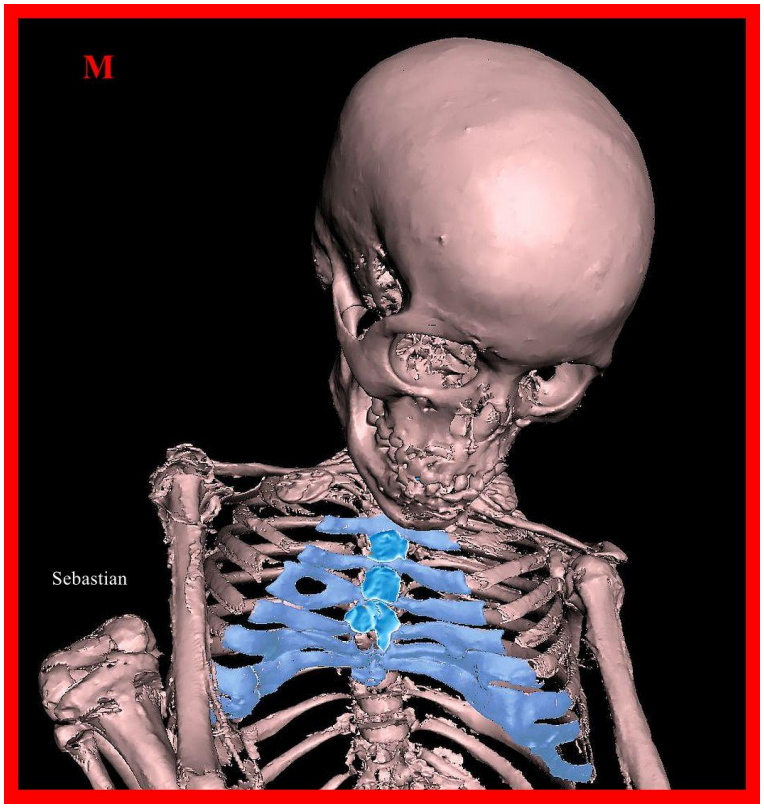

Figure 35: 3D CT of '***Sebastian***' showing the wide and depressed anterior chest wall containing unusually robust and distorted costal cartilages.

Figure 36: 3D CT showing '***Josefina***' with the air filled chest wall cavity *(in green)*.

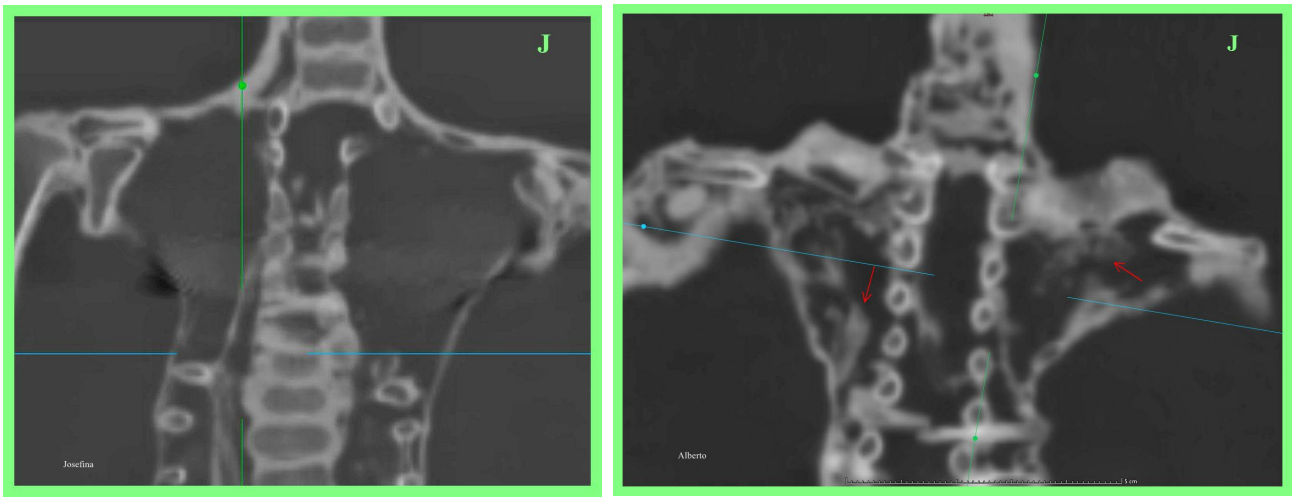

Figure 37: 2D CT coronal scans of '***Josefina***' *(left image)* compared with '***Alberto***' *(right image)*. Note the presence of irregular remnants *(red arrows)* within the thoracic cavity in '***Alberto***'.

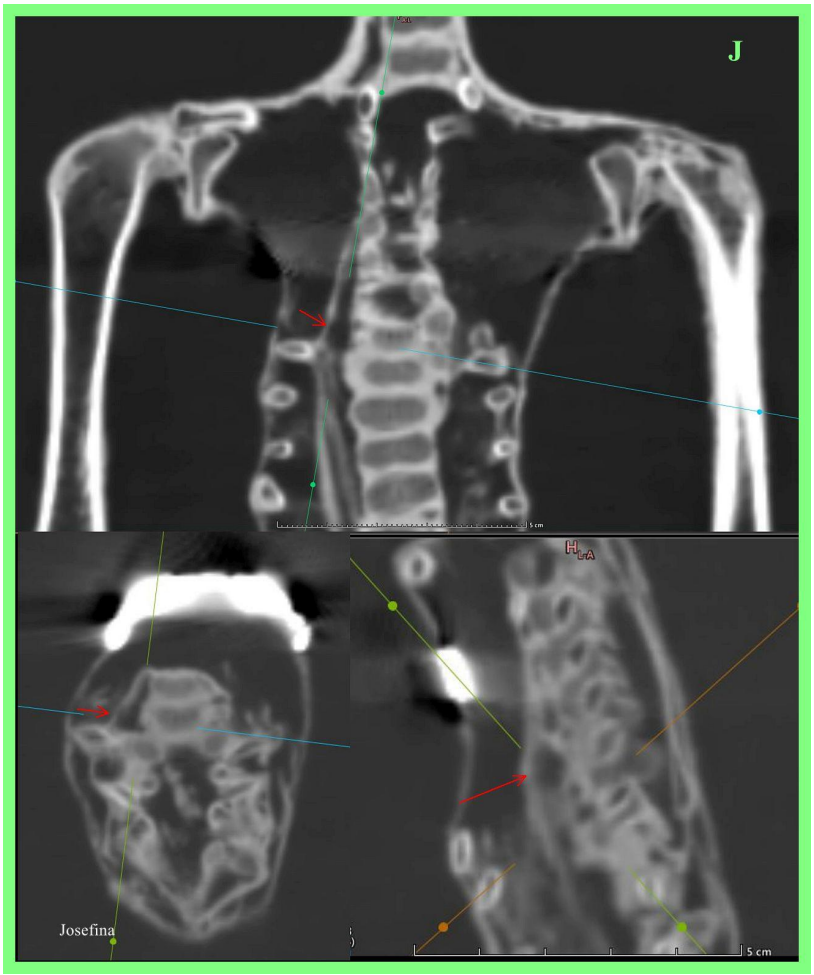

Figure 38: 2D CT scans with multi-planar reconstruction of the chest of '***Josefina***' showing presence of primitive tubular heart *(red arrow)* alongside the right side of spine. The aorta is seen extending downwards into the abdomen.

SECTION 6: ABDOMEN

M-type tridactyls:

- A prominent midline anterior abdominal fold is noted in the specimens. There is no evidence of navel. These are different from human.

•Solid organs are replaced by air-filled cavities leaving remnant of their capsule.

•Abundant coprolites are noted in bowels. A few small hyper-dense seeds can be found within.

•In '***Montserrat***', gravid uterus containing a single well-formed foetus is noted in the right side of the abdomen. The foetus is in breech presentation facing anteriorly and medially with right leg extended. Skull is partially collapsed with overlapping cranial bones. The limb bones, ribs and spine appeared to be crumbled together. There is suggestion of placenta on medial aspect of the uterus. The right side location of the gravid uterus is different from human which should be in midline. *(Figures 8,39)*

J-type tridactyls:

- Gastralia consisting of parallel horizontal robust ventral ribs (9 in '***Josefina***', 8 in '***Luisa***', 6 in '***Alberto***') is noted in anterior wall of the abdomen forming a strong bony shield. *(Figures 10,40)* The gastralia is connected to corresponding pairs of short ribs at the sides arising from the spine forming a robust horizontal triangular-shaped bony architecture. *(Figure 41)*

•2 pairs of additional floating ribs unconnected to gastralia are noted inferiorly.

•The posterior ends of short side ribs are attached to the thoracic spine. However some ribs are found with broken ends projecting into the thoracic spinal canal via the intervertebral foramina bilaterally in random fashion in all specimens. *(Figures 11,63,64)* This could have suggested a very strong crushing external compression force having been applied to the gastralia.

•On the right side, two parallel tubular structures are found extending from the thorax above to reach the abdomen alongside the spine below, suggestive of aorta medially and major vein laterally. There is suggestion of rudimentary tubular heart in lower part of the thorax in right paraspinal location. *(Figures 38,42)*

•The rest of the abdomen contains scattered remains. *(Figure 42)*

SECTION 6: ABDOMEN (contd.)

J-type tridactyls:

•Both '***Josefina***' and '***Luisa***' are found bearing 3 large eggs in their bulging pelvic abdomen below the gastralia. *(Figure 2)* These large eggs appear to be exceptionally dense on CT (density similar to metal implant). *(Figures 11,13)* With appropriate window settings for viewing, contents in these large eggs can be identified suggestive of embryos. *(Figure 43)* Large branching structures enveloping the anterior aspects of the large eggs were also noted, likely vascular in nature. 2 additional hyperdense tiny eggs can also be identified. *(Figure 44)*

•No eggs were found in '***Alberto***'.

•No navel nor median fold is noted in the anterior abdominal wall.

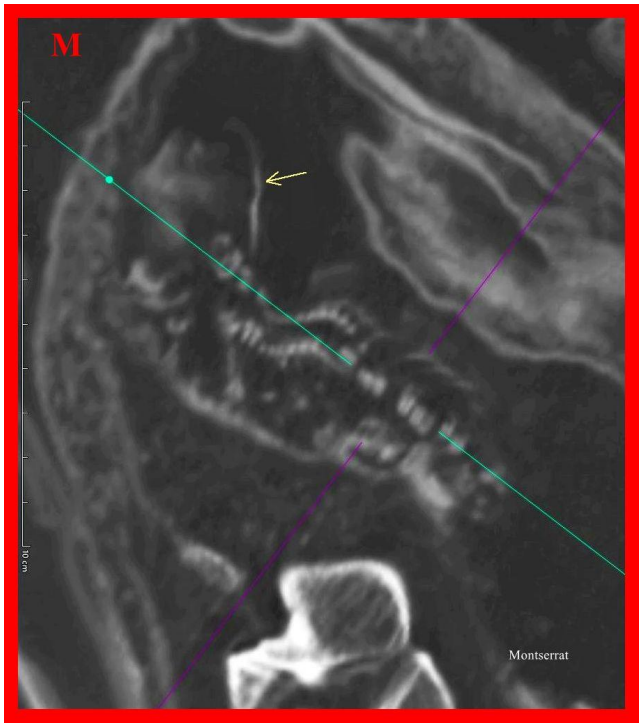

Figure 39: 2D CT scans with multi-planar reconstruction of '***Rafael***', the foetus inside the right side of the abdomen of '***Montserrat***' showing presence of collapse in the foetal spine. The foetal skull vault is marked *(yellow arrow)*.

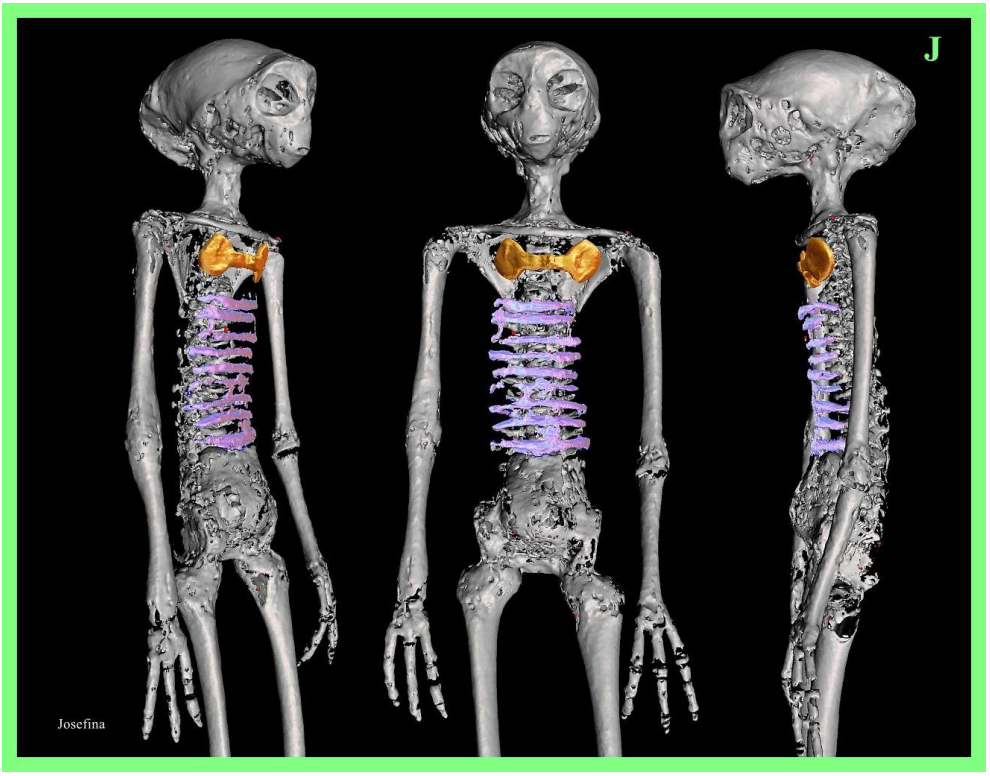

Figure 40: 3D CT of '***Josefina***' showing gastralia literally forming an armour protecting the anterior abdominal wall *(in pink)*. There is a dumbbell-shaped chest implant below the furcula *(in gold)*.

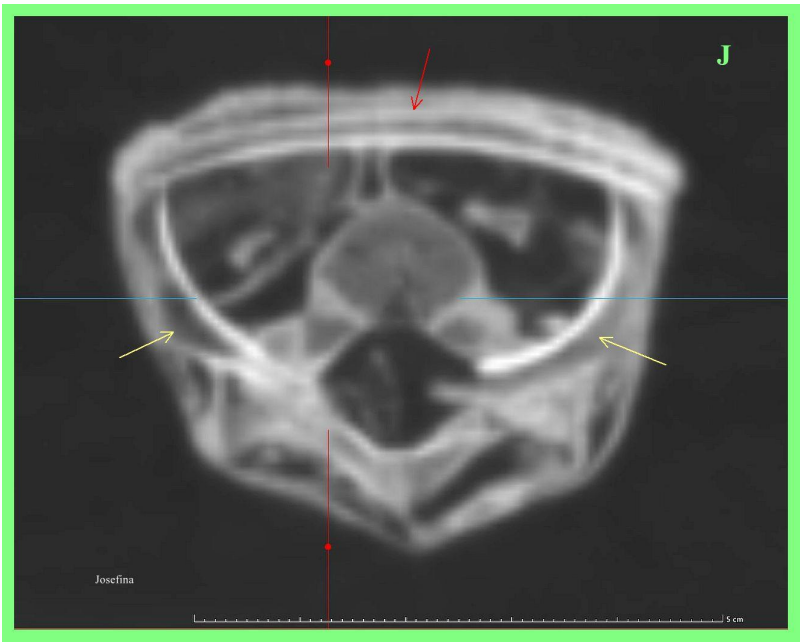

Figure 41: 2D axial CT scan of '***Josefina***' showing the ring of protection formed by the gastralia *(red arrow)* in front, short ribs *(yellow arrow)* at the sides and spine posteriorly.

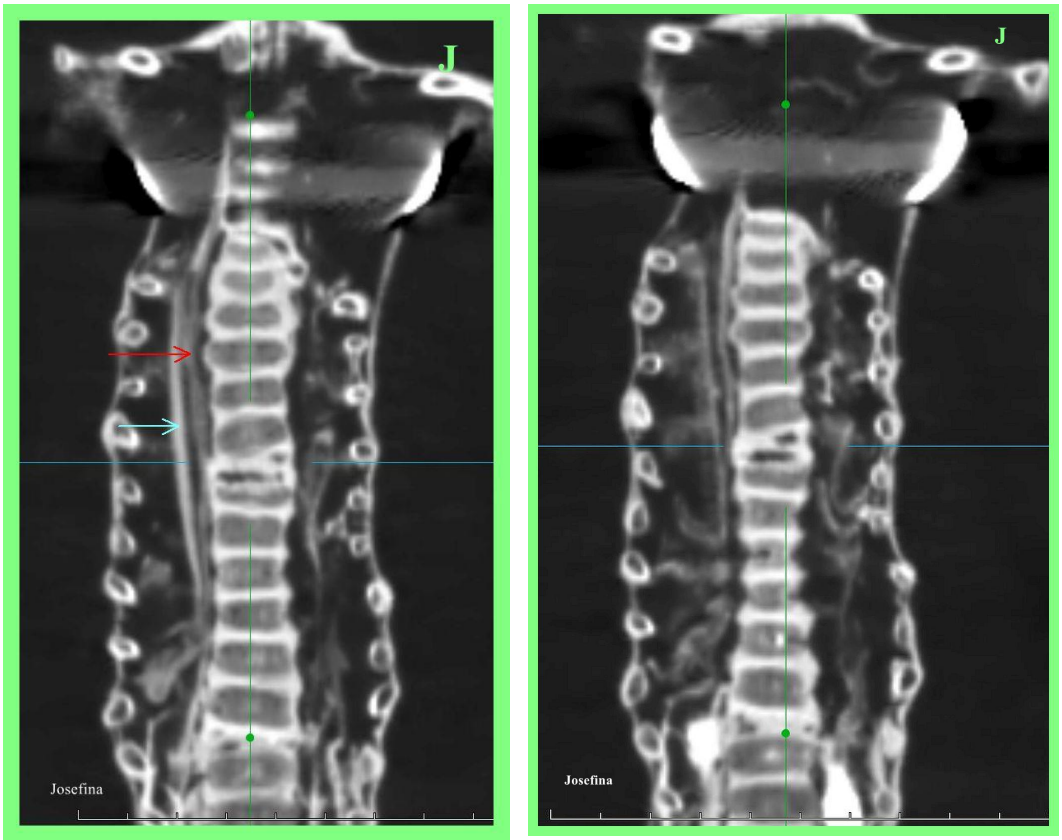

Figure 42: 2D coronal CT scan of the abdomen in '***Josefina***' showing presence of major artery *(red arrow)* and vein *(blue arrow)* alongside the spine *(left image)*. Scattered abdominal contents are also noted *(right image)*.

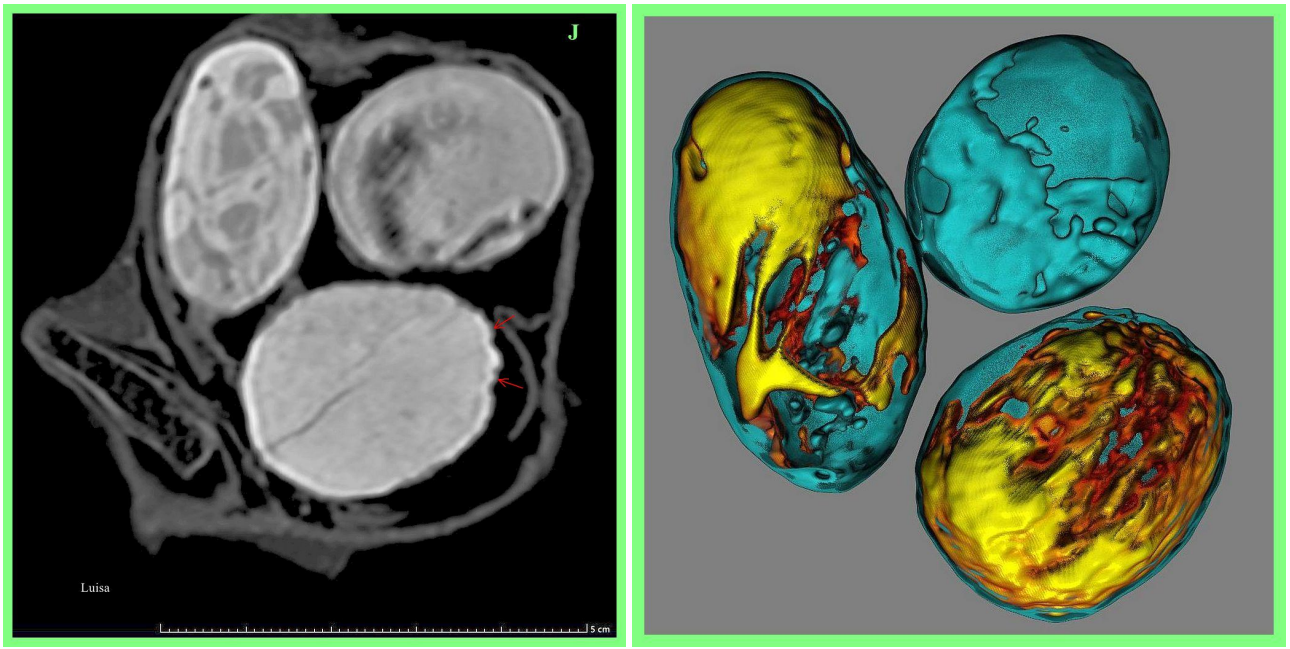

Figure 43: 2D coronal CT scan *(left image)* of '***Luisa***' showing the 3 large hyper-dense eggs. The shape of the eggs varies from roundish to oval. Thin and relatively more hyper-dense shells are noted showing wrinkling *(red arrows)* in the larger egg suggestive of soft shell. The eggs contain content of differential densities suggestive of embryos, best shown on 3D CT reconstruction *(right image)*.

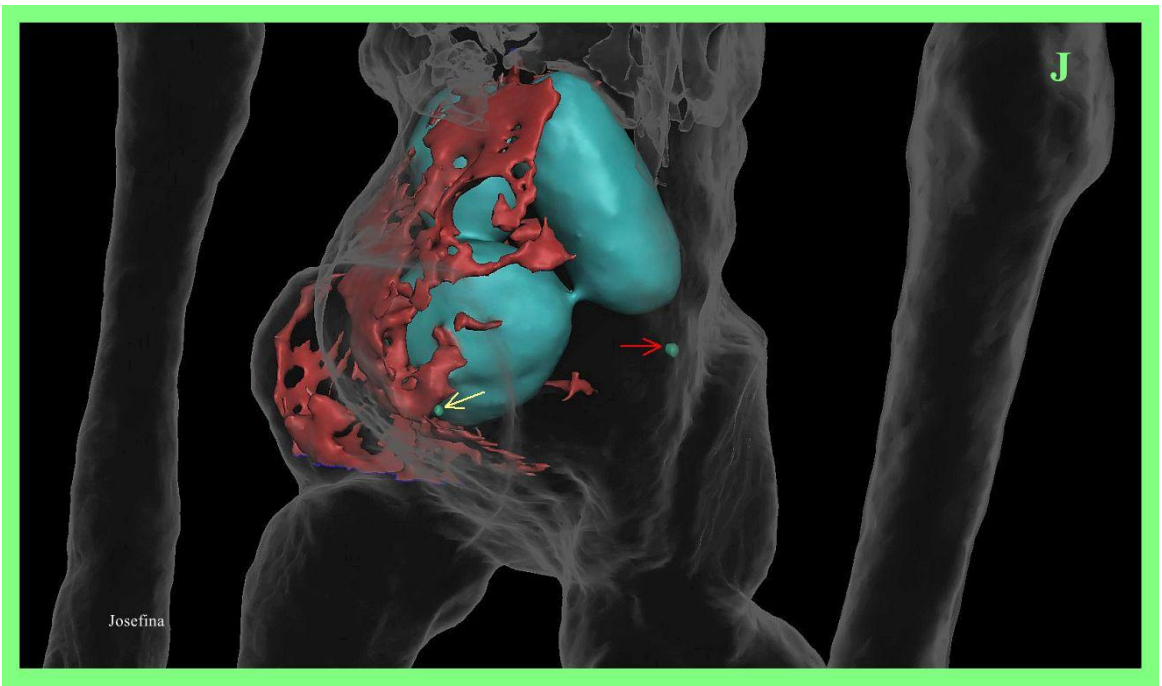

Figure 44: Left oblique view of 3D CT of '***Josefina***' showing skin in semi-transparency and presence of 3 large eggs in right side of the bulging pelvic abdomen, a tiny 4th egg in left side of pelvic abdomen *(red arrow)* and a tiny 5th egg in anterior lower pelvic abdomen *(yellow arrow)*. Large branching structures anterior to the eggs are noted, likely vascular in nature *(in red)*.

SECTION 7: SHOULDER GIRDLE

M-type tridactyls:

•The structures are similar to human consisting of bilateral scapulae unattached to spine or rib and bearing scapular spines and acromial processes articulating with the clavicles.

•As in human, the scapula bears shoulder joint articulating with humeral head.

•Medially, bilateral clavicles articulate with manubrium and sternum. *(Figure 45)*

J-type tridactyls:

• Quite different from M-type tridactyls, bilateral scapulae are large and aligned in a more coronal plane posteriorly, their medial edges being fused with the spinous processes of the upper thoracic spine. *(Figures 12,46)*

•The scapular spines attach bilaterally to furcula (similar to clavicles) but they join in the midline anteriorly by strong ligaments. *(Figure 45)*

•There is absence of manubrium nor sternum. There is no connection to the gastralia.

•The shoulder girdle appears to provide a triangular-shaped bone scaffolding offering robust stable support to the upper limbs and lungs.

•There is upward subluxation in the humeral heads in '***Josefina***' and '***Luisa***'. Extensive hematoma is noted in bilateral armpits of '***Luisa***'. *(Figure 12)*

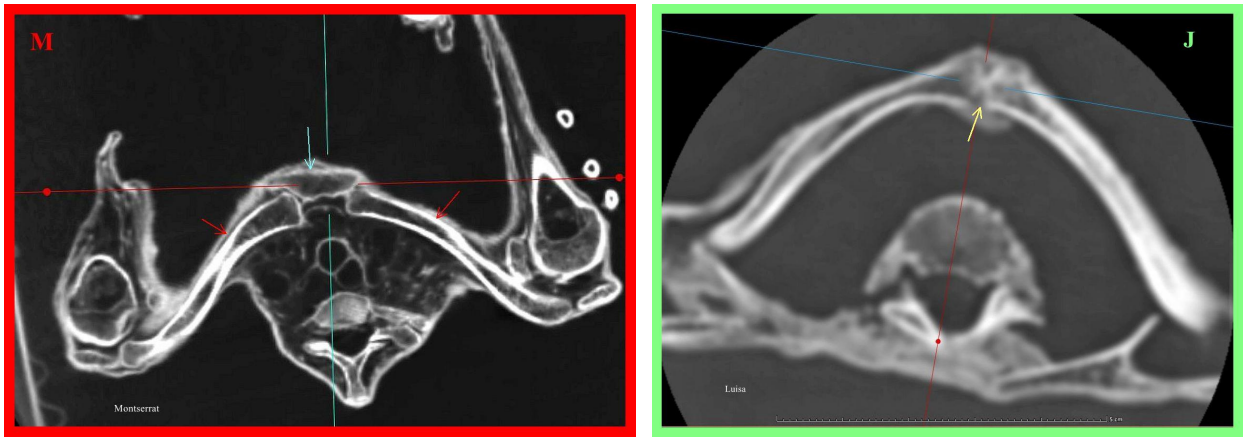

Figure 45: 2D axial CT scan of '***Montserrat***' *(left image)* showing bilateral clavicles *(red arrows)* joining manubrium in the midline *(blue arrow)*. 2D axial CT scan of '***Luisa***' *(right image)* showing furcula joining in midline *(yellow arrow)* with thickened capsule posteriorly.

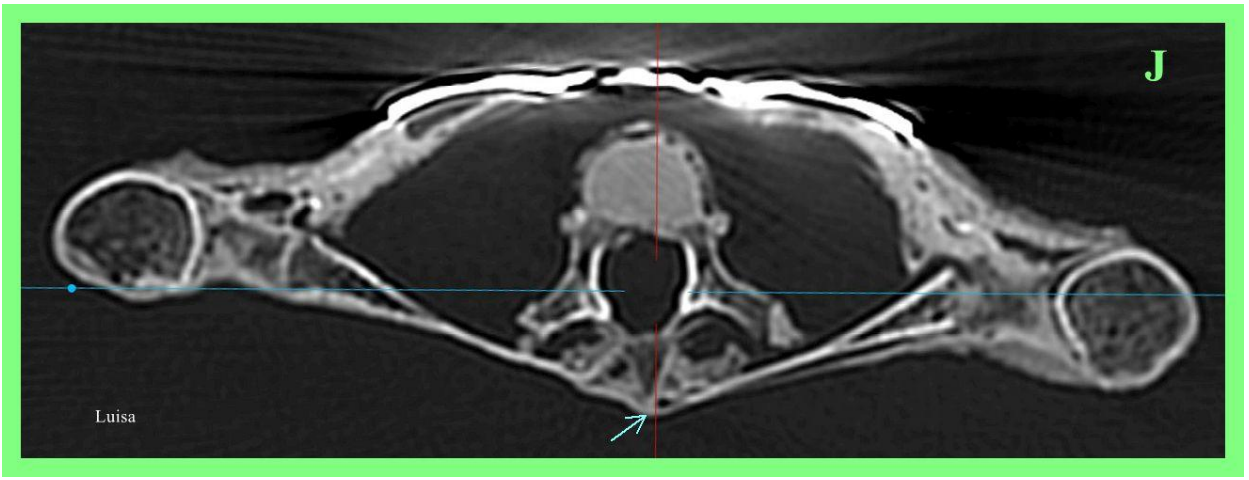

Figure 46: 2D axial CT scan of '***Luisa***' showing bilateral scapulae fused with the spinous process of thoracic spine.

SECTION 8: BONY PELVIS

M-type tridactyls:

•There is ring-shaped bony pelvis show similar configuration with human with presence of sacro-iliac joints and symphysis pubis.

•Hips joints are similar to human with ball-and-socket joints in acetabulum. Angled femoral necks are noted.

J-type tridactyls:

• Quite different from M-type tridactyls, there is an H-shaped pelvic girdle formed by 2 vertical flaring flat rectangular-shaped vertical bones on either sides articulating centrally with the lowest 3 vertebrae via vertical joints similar to sacro-iliac joints. There are no anterior elements such as pubic bones nor symphysis pubis. There are significant individual variations in the degree of upward flaring of the pelvic bones and showing asymmetry between the right and left sides. *(Figures 48,49,50,51)*

•The hips are completely different from the M-type tridactyls. There are large upward pointing upper femoral epiphyses in '***Josefina***' and '***Alberto***' but absent femoral epiphysis in '***Luisa***'. There is no distinct femoral neck. Despite the large size of the upper end of femur, only a small part of it articulates with the inferior edge of the pelvic bone. The joint appears to be orientated in an antero-posterior direction showing thick joint capsule. *(Figures 13,49,50)*

•There is evidence of injury in the lateral part of the right upper femoral epiphysis in '***Alberto***'. A metallic implant could be seen fused with the detached bone fragment. There is distortion in the shape of pelvic bone and deviation in lower end of spine toward the left side suggestive of old injury with bony remodelling. *(Figure 50)*

Figure 47: 3D CT of '***Montserrat***' showing bony pelvis and both hips in flexion . Note the female type of pelvis similar to human.

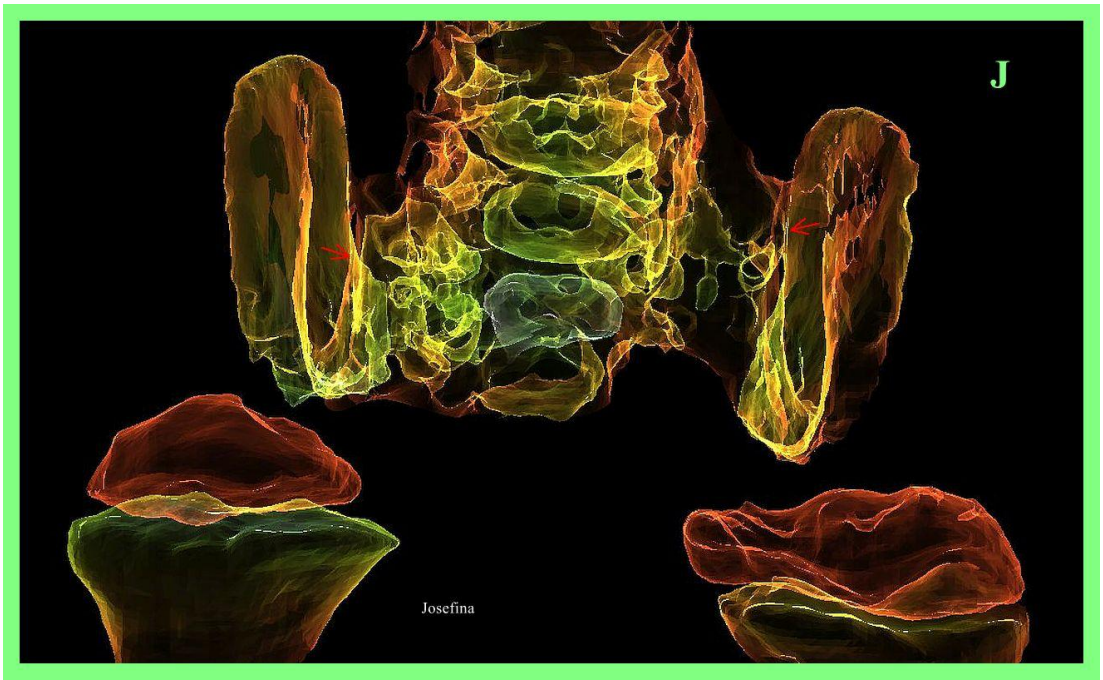

Figure 48: 3D CT of '***Josefina***' in semi-transparency showing the lower 3 vertebrae are connected to the vertical pelvic bones via sacro-iliac joints *(red arrow)* forming an H-shape configuration of the pelvic girdle, lacking the anterior component. The hips joints are located inferiorly and orientated in an antero-posterior direction.

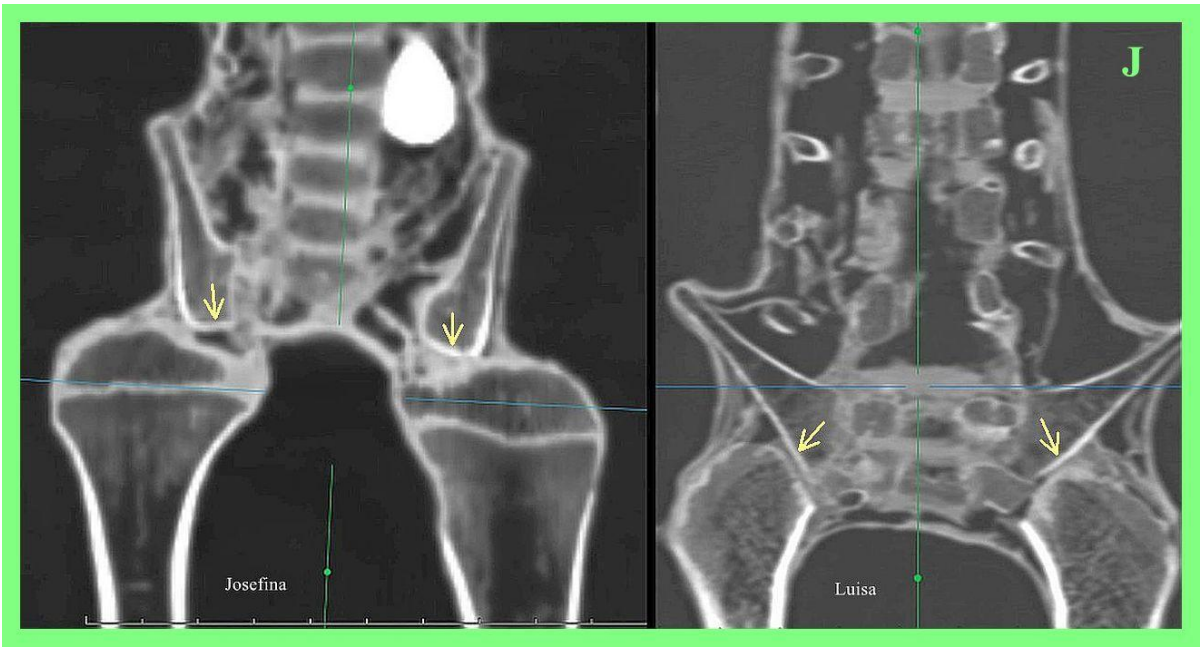

Figure 49: 2D coronal CT showing the hip joints *(yellow arrows)* of '***Josefina***' *(left)* and '***Luisa***' *(right)*. Note the large upper femoral epiphysis located superiorly in '***Josefina***'. Instead, in '***Luisa***' there is absence of epiphysis with wear and tear noted in the articulating surface of left femur

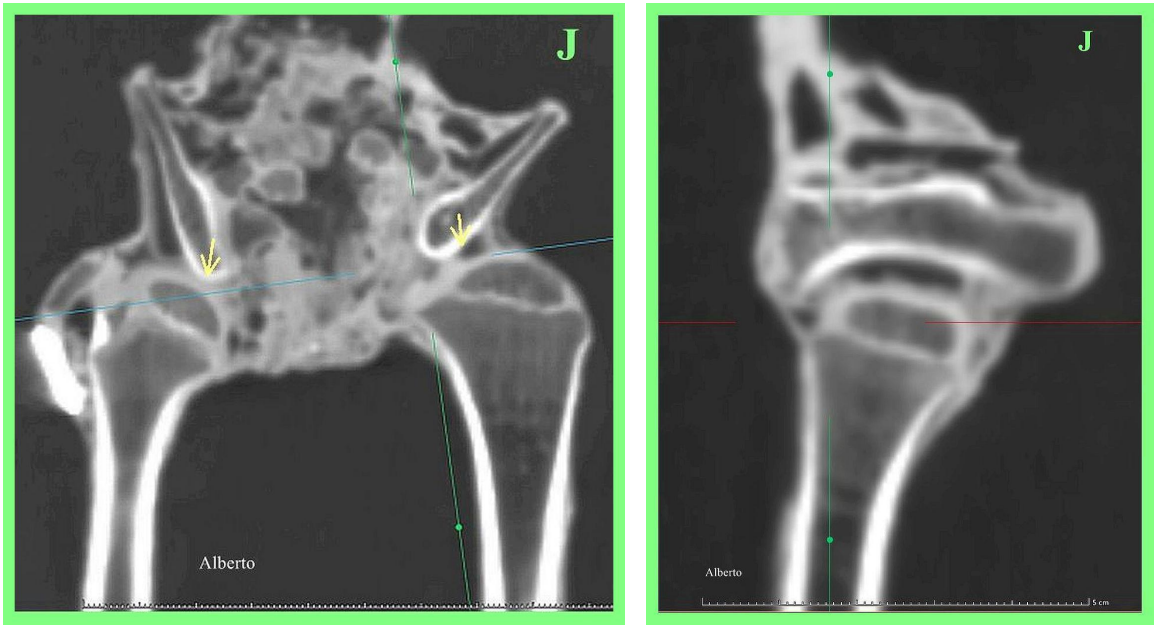

Figure 50: 2D coronal CT of '***Alberto***' *(left image)* showing subcutaneous metallic implants overlying the upper right femur. There is evidence of injury in lateral part of upper femoral epiphysis and resultant bony healing of the detached bone fragment associated with the metal implant. Note the uneven levels of the hip joints *(yellow arrows)* and the variation in flaring in the left pelvic bone suggestive of stress remodelling of bones. 2D sagittal CT scan *(right image)* showing the antero-posterior orientation of the right hip joint in '***Alberto***'. Note the thick joint capsule anteriorly.

SECTION 8: LIMBS

M-type tridactyls:

•Relative bony proportions in upper and lower limb long bones remain similar to human. Paired forearm and leg bones are present with similar morphology including presence of patellae. Achilles tendon can be found. *(Figure 51)*

•In the carpal bones of '***Maria***', there is carpal bone coalition with the diminished-sized trapezium and trapezoid bones fused by bony union. Together they articulate with the lateral digit. The capitate articulates with the middle digit. The hamate articulates with the medial digit. In '***Montserrat***' the trapezium and trapezoid bones are absent. The scaphoid articulates directly with the lateral digit. The capitate articulates with the middle digit. The hamate articulates with the medial digit. The lunate, triquetrum and pisiform remain similar to human anatomy. *(Figure 54)*

• Tridactyl is the hallmark in this group. Symmetrically and well spaced 3 equally long finger digits covered with skin, each bearing 4-5 separate segments ('***Maria***' 5; '***Montserrat***' and '***Sebastian***' 4) are found articulating directly with the carpal bones. There is absence of metacarpals nor related soft tissue forming the palm. *(This differs from the asymmetrical configuration in human that have 5 metacarpals in the palm bearing two-segment thumb and four fingers of unequal lengths each having 3 segments)* *(Figure 53)*

•In the hindfoot, all components of tarsal bones (including talus, calcaneum, navicular, cuboid, 3 cuneiforms) are present in similar alignment as human. There is evidence of plantar fascia and ligaments. Plantar arch is present. There is absence of metatarsals and related soft tissue composing the forefoot. 3 symmetrical well spaced elongated toe digits of similar length, each bearing 3-4 segments ('***Maria***' and '***Montserrat***' 4; '***Sebastian***' 3), are found articulating directly with tarsal bones. *(Figure 55,56)*

•Crawl-deformities are noted in distal parts of some digits in the feet. Soft tissue contact cushion pads are noted in plantar pressure points on digits. *(Figure 55)*

SECTION 8: LIMBS (contd.)

J-type tridactyls:

- A significant difference with M-type tridactyls or human is the findings of single forearm and leg bones instead of pair bones. *(Figure 51)*

- The limb bones show difference in proportion with relatively long upper limb bones. Proximal bones are relatively long as compared with distal bones. *(Figure 51)* The internal bony architecture remains similar to M-type tridactyl or human *(unlike hollow bone of birds)* with presence of bone marrow at either ends and relatively empty central shaft with thick cortex. *(Figure 52)*

- The shape of long bones are different with flaring more distally showing an Erlenmeyer flask appearance. *(Figure 51,52)*

- In the hand with the tridactyl configuration, 3 symmetrically arranged widely separated long fingers each bearing 4 separate segments are found articulating symmetrically with a single slab-like carpal bone.

- In the knee, a cushion-like soft tissue is seen wedged between the bone surfaces. No evidence of patella is noted. *(Figure 52)*

- In '***Josefina***' the distal end of leg bone extend further into a lateral tubercle distally alongside a single tarsal bone. In '***Luisa***' and '***Alberto***', the lower ends of leg bones are flat and end abruptly articulating with a flat slab-like single rectangular-shaped tarsal bone. The foot is flat with the tarsal bone bearing 3 symmetrically placed widely separated digits each bearing 2-3 separate segments (3 in '***Josefina***' and '***Luisa***', 2 in '***Alberto***'). *(Figure 52,55)*

- No evidence metacarpals or metatarsals nor associated palm and forefoot are present.

- Reptilian patterned skin texture can be seen in foot in '***Luisa***'. *(Figure 55)*

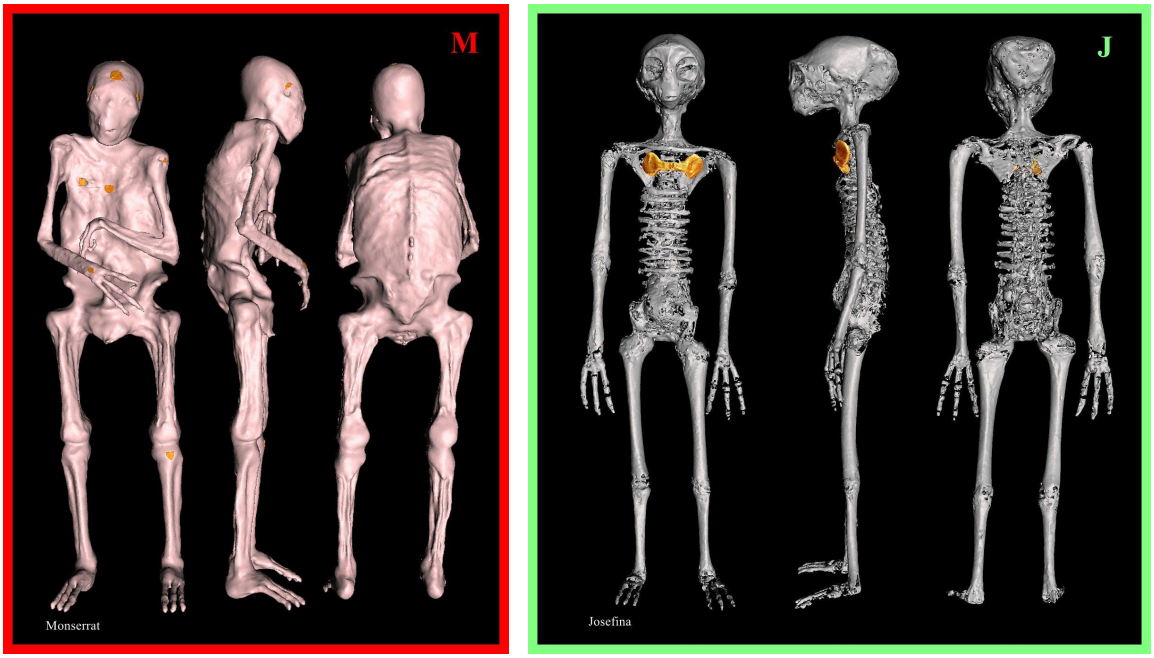

Figure 51: 3D CT of '***Montserrat***' reformed with extended legs *(left image)* showing paired forearm and leg bones. The proximal and distal long bones are of similar lengths. 3D CT of '***Josefina***' *(right image)* showing single forearm and leg bones. Note the disproportionately longer proximal bones.

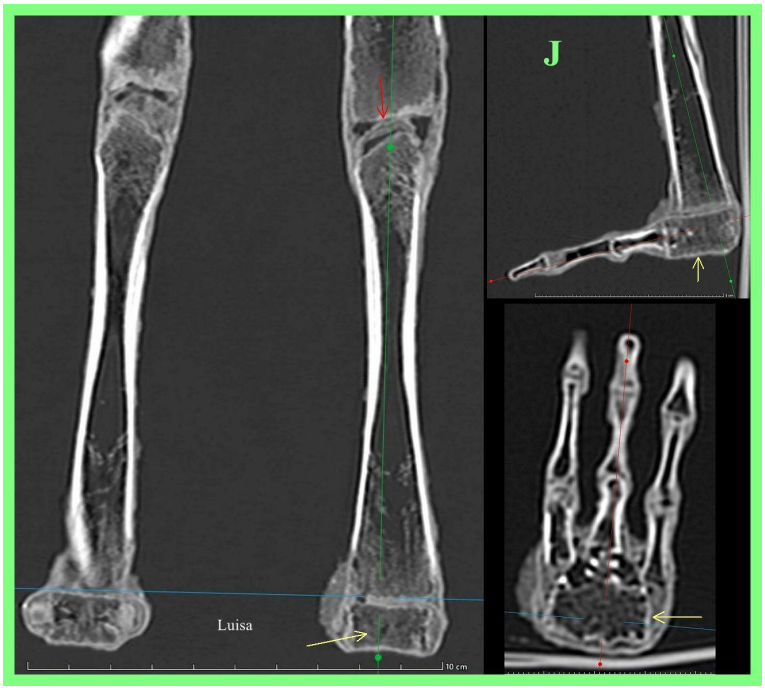

Figure 52: 2D CT scans in coronal *(left)*, sagittal *(right upper)* and axial *(right lower)* projections showing left leg and foot of '***Luisa***'. A structure reminiscent of meniscus *(red arrow)* can be seen in left knee. Note the slab-like rectangular-shaped single tarsal bone *(yellow arrow)*. With correct window setting on CT, the long bone basically resembles M-type tridactyls or human bone showing bone marrow at either ends and 'empty' central shaft due to marrow fat. The distal long bones showing smooth widening at their distal ends resembling Erlenmeyer flask appearance.

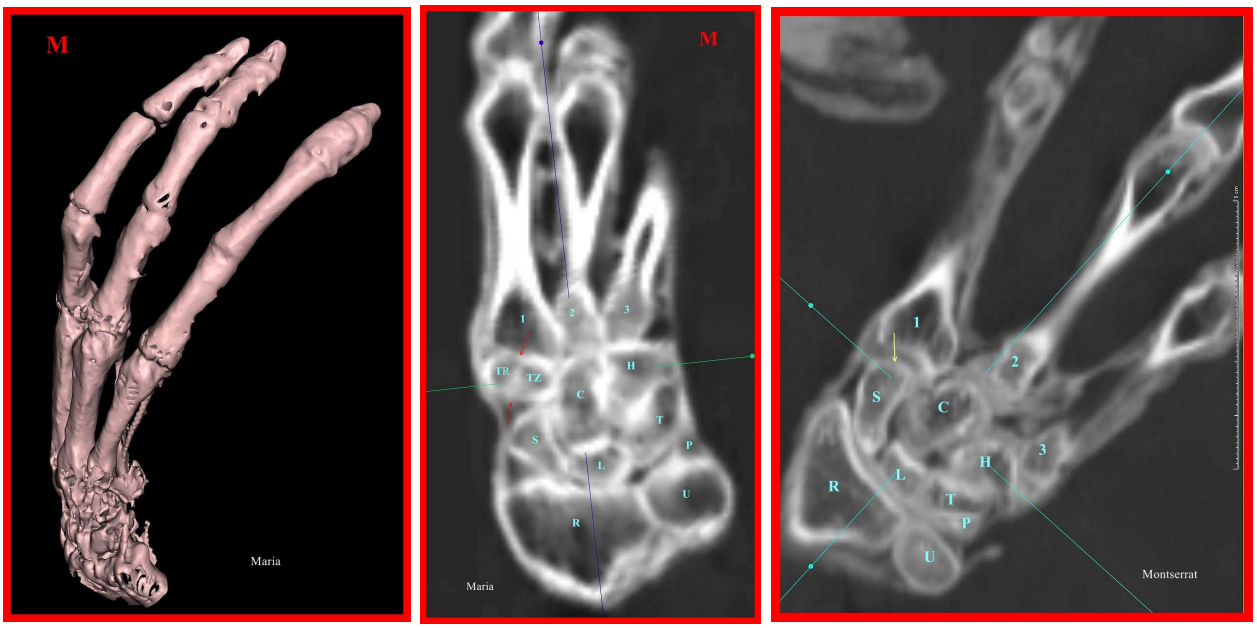

Figure 53: 3D CT of right hand of '***Maria***' *(left image)* showing tridactyl with very long digits bearing 5 segments. Multiplanar reconstruction of 2D CT scan showing details of carpal bones of '***Maria***' *(middle image)* . Carpal coalition with fused hypoplastic trapezium and trapezoid *(red arrows)* are noted articulating with the lateral digit. The rest of carpal bones are intact. Multiplanar reconstruction of 2D CT scan of wrist of '***Montserrat***' *(right image)* show absence of trapezium and trapezoid with the scaphoid *(yellow arrow)* articulating directly with the lateral digit. Other carpal bone remain intact. *(R=radius, U=ulna, S=scaphoid, L=lunate, T=triquetrum, P=pisiform, TR=trapezium, TZ=trapezoid, C=capitate, H=hamate, 1=lateral digit, 2=middle digit, 3=medial digit)*

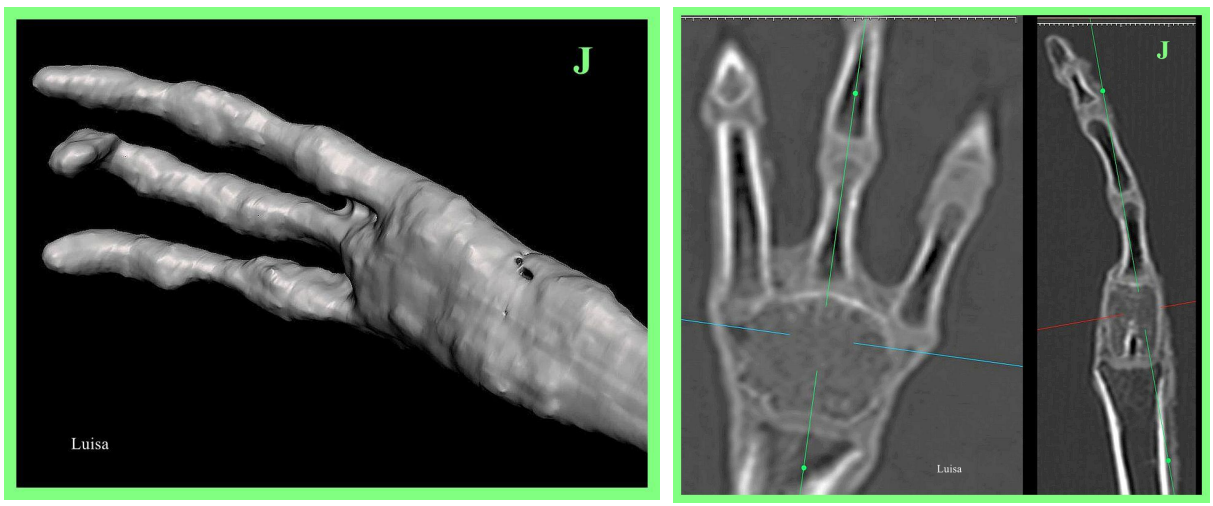

Figure 54: 3D CT of left hand of '***Luisa***' *(left image)* showing tridactyl digits with 4 separate segments. Note the flat rigid carpal area. 2D CT scans *(right image)* show presence of single polygonal slab-like carpal bone with symmetrical alignment of digits.

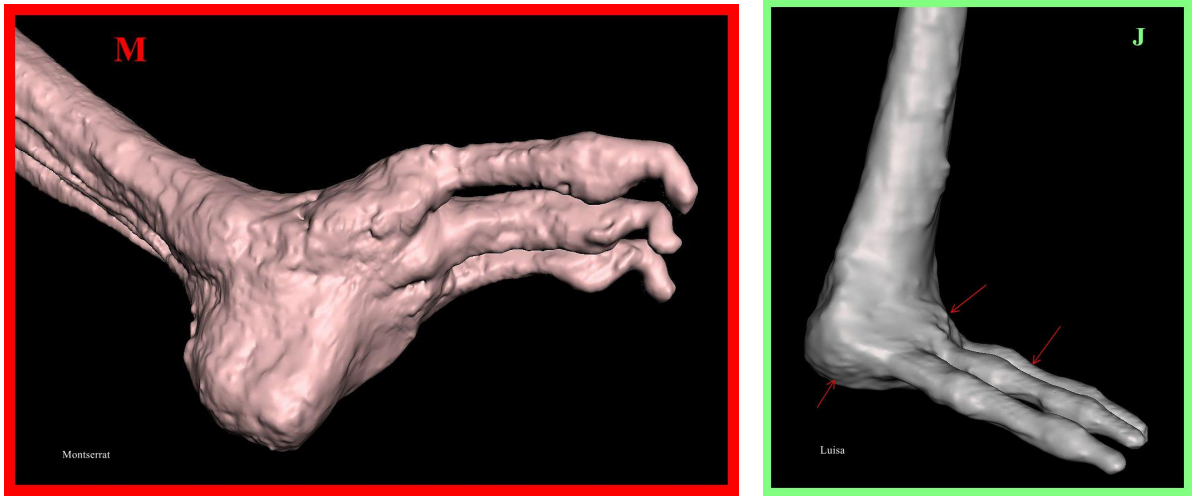

Figure 55: 3D CT of left foot of '***Montserrat***' *(left image)* showing tridactyl digits with 4 separate segments. Note the crawl deformity and contact pads in distal digits and presence of plantar arch. 3D CT of left foot of '***Luisa***' *(right image)* showing flat foot and tridactyl digits with 3 separate segments. Note the reptilian skin *(red arrows)* on the heel and digits.

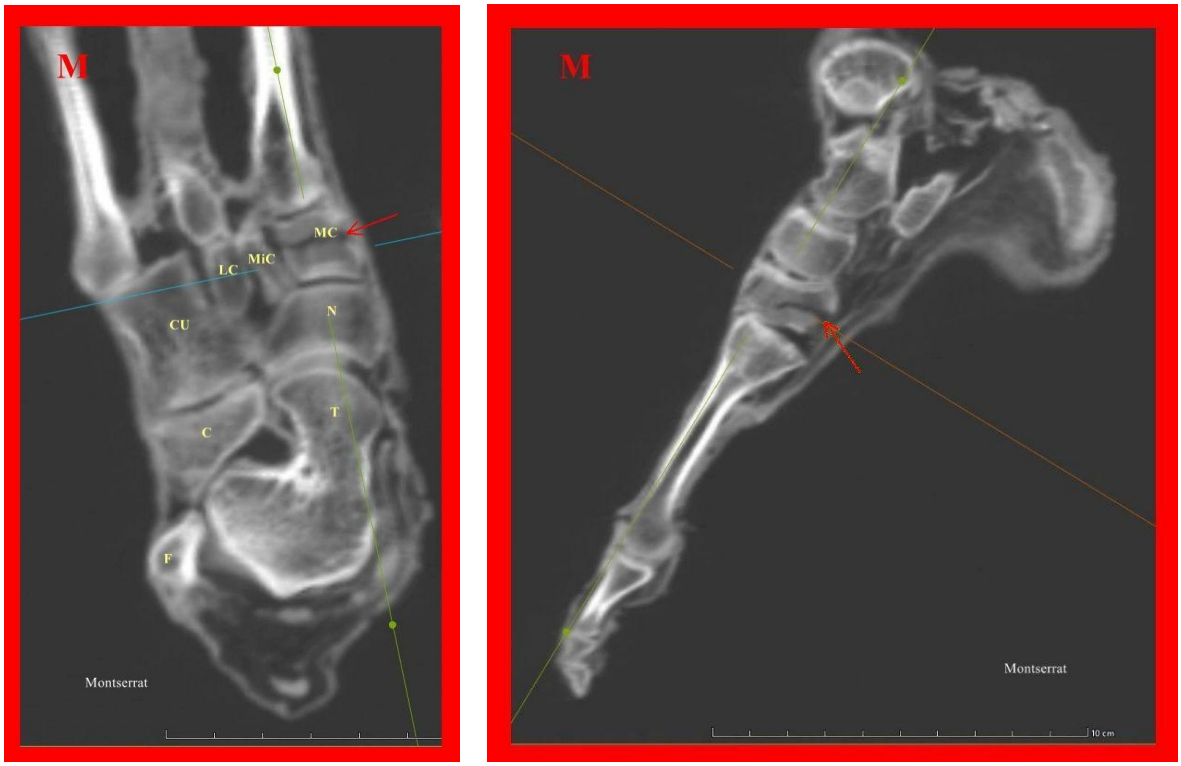

Figure 56: 2D axial *(left image)* and sagittal *(right image)* CT scans of right foot of '***Montserrat***' showing complete set of tarsal bones similar to human. Note the fracture *(red arrows)* in medial cuneiform. *(F=fibula T=talus C=calcaneum N=navicular CU=cuboid MC=medial cuneiform MIC=middle cuneiform LC=lateral cuneiform)*

SECTION 9: SPINE

M-type tridactyls:

- The spine is essentially similar to human with cervical, thoracic, lumbar and sacral segments. The lower half of sacrum in '***Maria***' is truncated due to injury. There is an extended 5th sacral segment in '***Montserrat***' without separate coccygeal segments. '***Sebastian***' had a tiny inconspicuous coccygeal segment(s). *(Figure 57)*

- Evidence of diseases including osteolytic bone secondaries due to disseminated cancer and degenerative bone changes are found in thoracic spine of '***Maria***'. Evidence of trauma including rotary subluxation of cervical vertebra is found in '***Sebastian***'. *(Figure 57)*

- Contrary to findings in '***Maria***' and '***Montserrat***', generalised calcified intervertebral disks are noted in '***Sebastian***'; the finding being extremely unusual in human. *(Figure 57)*

- The spinal canal is essentially similar to human.

- The foramen magnum and the cranio-vertebral junction including atlas of C1 and axis of C2 remain similar to human. *(Figure 23)*

J-type tridactyls:

- The spine featured unprecedented anatomy that is completely different from M-type tridactyls. There are differences amongst the different specimens of J-type tridactyls. All had hyper-dense and thick intervertebral disks. There is a total of 22-25 segments in the spine.

- There are isolated compression fractures, subluxation and disk protrusion in all specimens. *(Figures 61,62)* One possibility is that massive compression force on the gastralia had led to rib fractures as well as trauma to the spine in all 3 specimens.

- The cervical spine shows quite variable segments. '***Josefina***' has 4 segments only. '***Luisa***' has 6 segments and '***Alberto***' has 9 segments. The cervical vertebra show simple ovoid shape with minimal posterior elements lacking posterior spinal arch. However, the intervertebral distance are not constant. *(Figure 58)* There is great difference in the length of the neck. *(Figure 2)* A postulation is that the neck is extensible, presumably by means of hydraulic pressure through venous engorgement. *(Figure 34)* The thick skin on the neck may be elastic and could have provided supportive function serving as exoskeleton, whereas the cervical vertebrae may only serve the purpose of preventing collapse of the spine.

SECTION 9: SPINE (contd.)

J-type tridactyls:

- There is lack of atlas/axis/odonotid arrangement in cranio-vertebral junction, contrary to the M-type tridactyls. The first cervical vertebra is rounded and fits into the roundish ring of bone in the foramen magnum. *(Figures 24,58,63)*

- '***Josefina***' and '***Alberto***' share similar morphology in the thoracic spine that is completely different from '***Luisa***'. Whereas '***Luisa***' has conventional looking vertebral bodies, '***Josefina***' and '***Alberto***' have upper thoracic vertebrae that show a ladder-like pattern with horizontal bar-like anterior bony components replacing the vertebral bodies, leaving gaps in between. Lower thoracic vertebrae are relatively robust and fused. *(Figures 59,60)*

- The sacral segments in '***Josefina***' and '***Luisa***' are located posteriorly whereas in '***Alberto***' the sacral spine is located anteriorly just beneath the anterior abdominal wall. *(Figures 61)*

- There is apparent lack of spinal canal in the cervical spine. An extremely spacious spinal canal is found below the thoracic spine with undiminished diameter extending to the lower end of the spine ending abruptly with wide opening of spinal canal, covered by thin skin only. *(Figures 61,62)* Superiorly, the spinal canal tapers to a blind end at level of the lowest cervical vertebra. As have been mentioned, isolated fractured ribs are seen projecting into the spinal canal via intervertebral foramen. There are other soft tissue debris within the spinal canal. *(Figures 11,66)*

- A structure resembling spinal cord can be seen projecting into the foramen magnum in '***Josefina***'. It runs close to posterior surfaces of cervical vertebrae. *(Figure 63,64)* It enters the spacious spinal canal posteriorly at level of lowest cervical vertebra. At upper thoracic spinal canal, it then loops forward and become attached to the back of the anterior component of the first thoracic spine. From this point, it divides into 2 parallel strands extending retrogradely in a straight line obliquely upwards and anteriorly above the first thoracic segment to become attach to the soft tissue of anterior lower neck near midline. *(Figures 64,65)* This arrangement of the spinal cord is completely unprecedented and not found in M-type tridactyls.

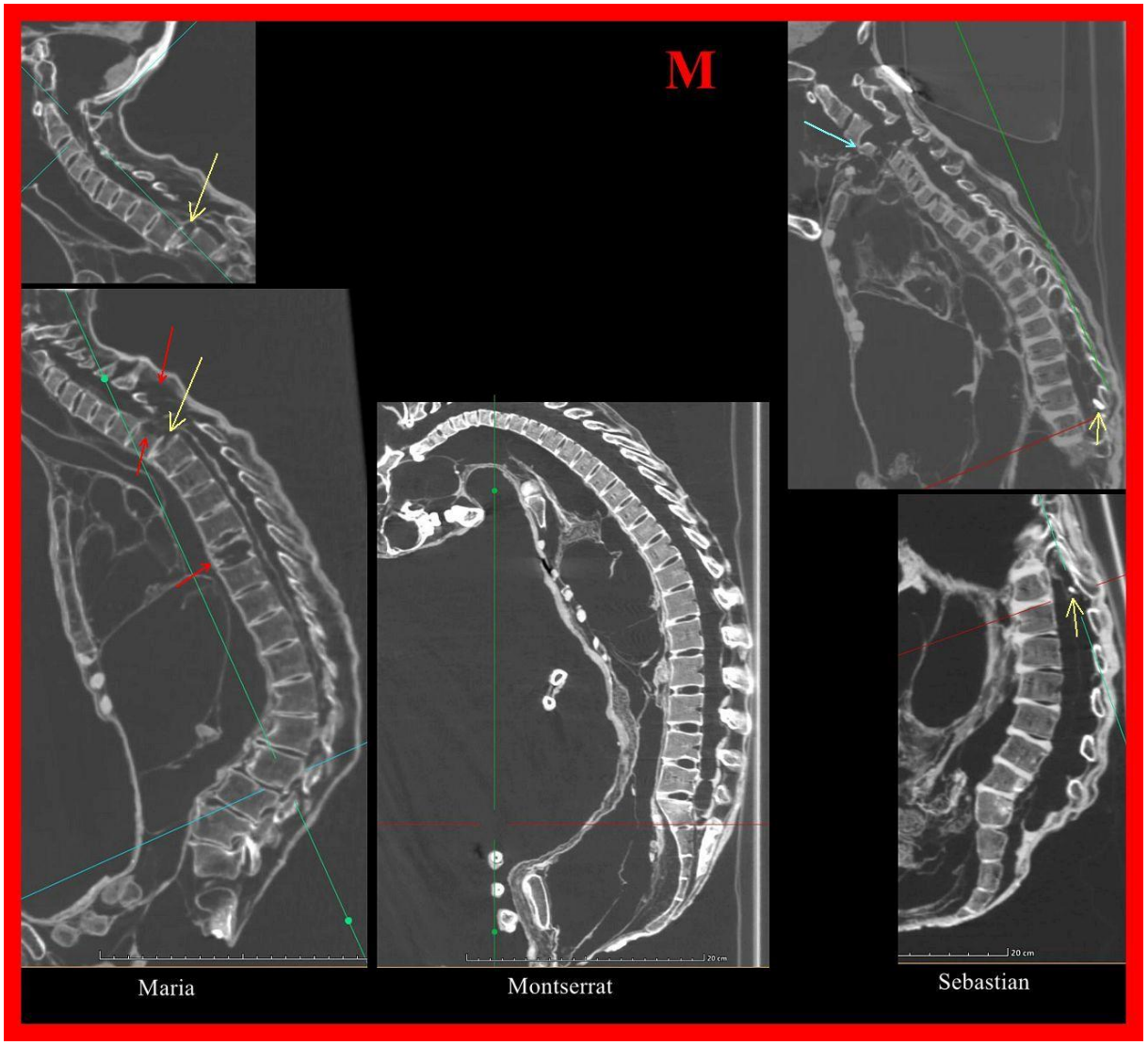

Figure 57: 2D sagittal CT scan of the spine of '***Maria***' *(left image)*, '***Montserrat***' *(middle image)* and '***Sebastian***' *(right image)* basically resembling human skeleton. Upper images are better aligned for the cervical spine due to tilting with corresponding location marked *(yellow arrows)*. Note the unusually dense intervertebral disks in '***Sebastian***', not found in '***Maria***' and '***Montserrat***' and not a feature in human. The lower sacral segments in '***Maria***' had been truncated and showing a small metal implant. Osteolytic bone lesions are noted in thoracic spine of '***Maria***'. *(red arrows)* Rotary subluxation is noted in cervical spine of '***Sebastian***'. *(blue arrow)*

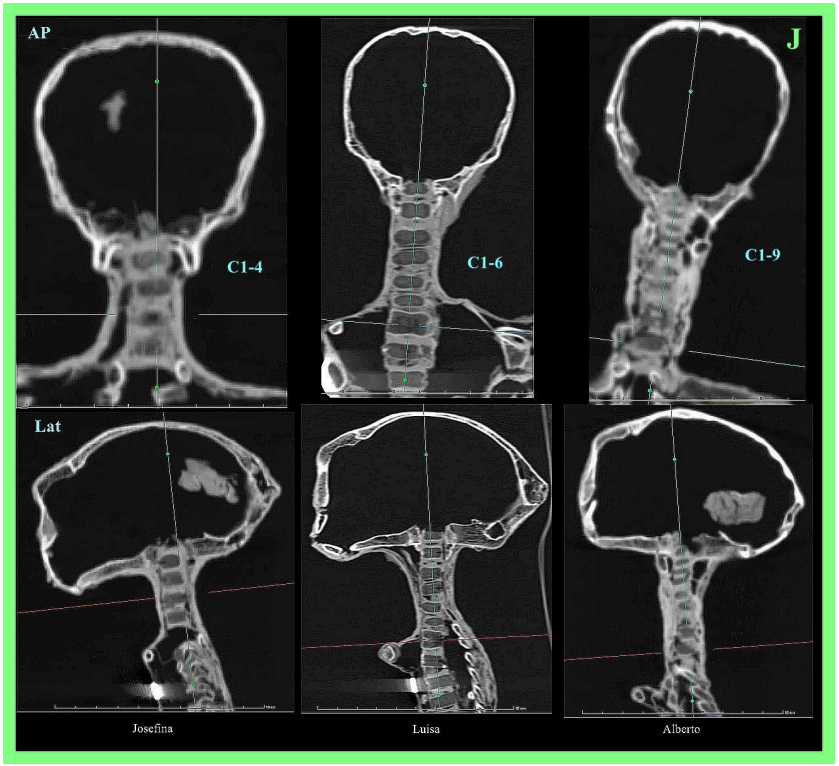

Figure 58: 2D coronal *(upper)* and sagittal *(lower)* CT scans of the cervical spines of '***Josefina***' *(left images)*, '***Luisa***' *(middle images)* and '***Alberto***' *(right images)* showing variable length of neck, variable number of cervical vertebrae, variable distances between vertebrae, lack of posterior spinal elements and lack of atlas/odontoid/axis configuration in foramen magnum.

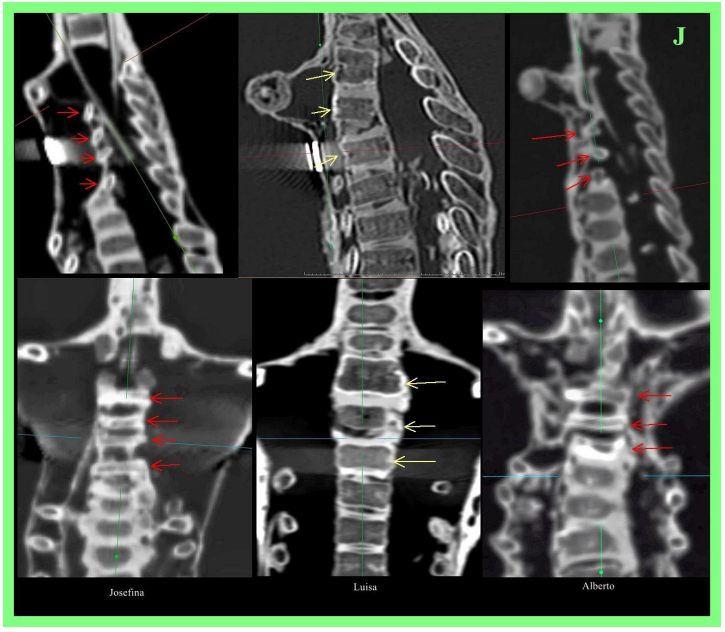

Figure 59: 2D sagittal *(upper images)* and coronal *(lower images)* CT scans of the thoracic spine of '***Josefina***' *(left images)*, '***Luisa***' *(middle images)* and '***Alberto***' *(right images).* The vertebral bodies in '***Luisa***' *(yellow arrow)* are prominent and conventional but in '***Josefina***' and '***Alberto***', the upper thoracic vertebrae *(red arrows)* are completely different with the vertebral bodies being replaced by narrow bar-shaped structures with gaps in between resembling a ladder. There is wide gap between the cervical spine and the uppermost thoracic vertebra although the posterior elements remain intact.

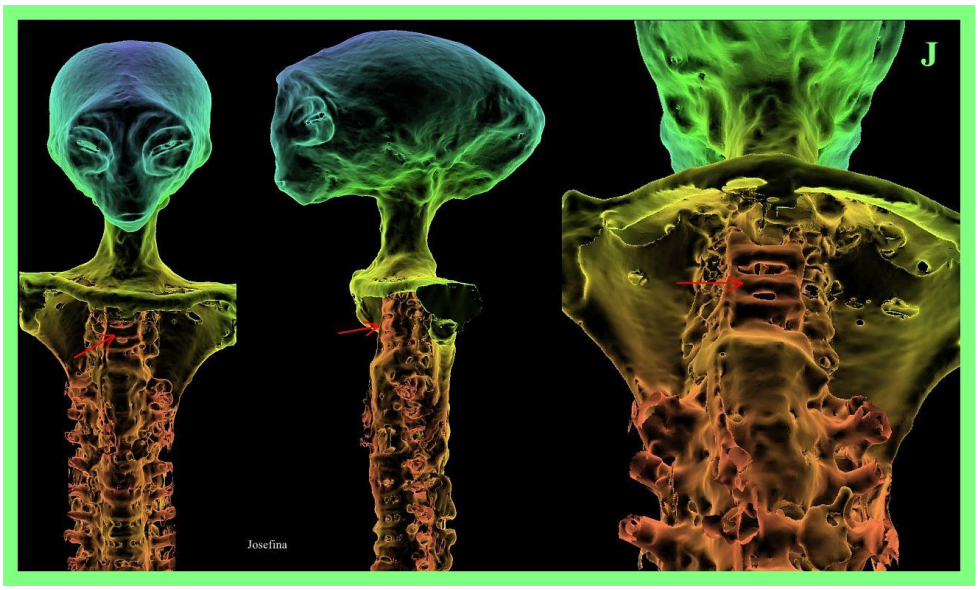

Figure 60: Digitally dissected 3D CT of thoracic spine of '***Josefina***' in frontal *(upper image)*, lateral *(middle image)* and tilted frontal view *(right image)* showing unconventional anatomy with vertebral bodies in upper thoracic spine being replaced by narrow bar-shaped bony structures *(red arrows)* with gaps in between. There is wide gap between the cervical spine and the uppermost thoracic vertebra although the posterior elements remain intact. The lower thoracic vertebrae appear to be fused and robust.

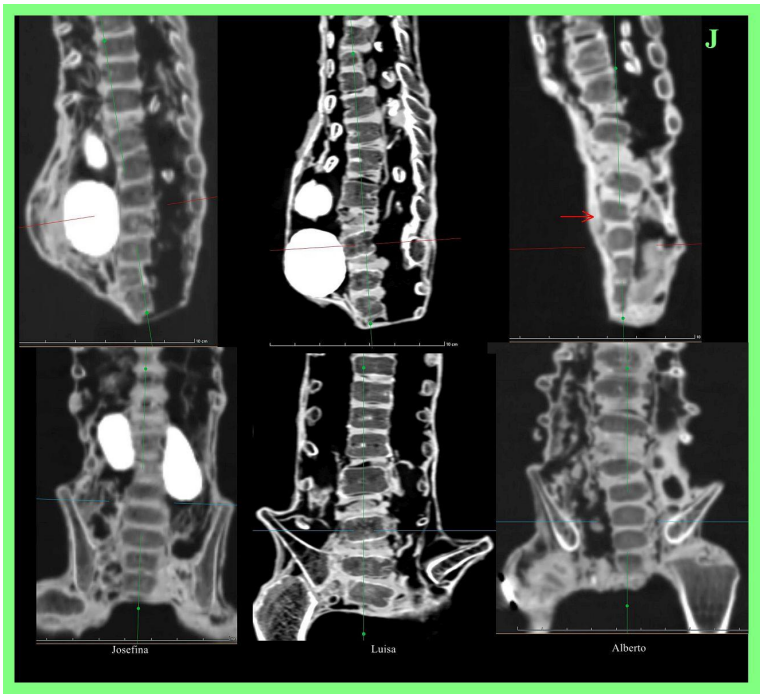

Figure 61: 2D sagittal *(upper images)* and coronal *(lower images)* CT scans of the sacral spines of '***Josefina***'*(left images)*, '***Luisa***'*(middle images)* and '***Alberto***'*(right images).* Note the extremely wide spinal canal that remains open and ending abruptly below covered by thin skin, unlike the tapering anatomy in M-type tridactyls or human. Note the peculiar anatomy in '***Alberto***' where the sacral spine is immediately under the anterior abdominal wall. *(red arrow)* Asymmetrical flaring of bony pelvis is noted in '***Luisa***' and '***Alberto***'. The is evidence of bony injury with healing and presence of metal implant in right hip of '***Alberto***'.

Figure 62: 2D sagittal CT scans of the spines of '***Josefina***' *(left image)*, '***Luisa***' *(left middle image)* and '***Alberto***' including enlarged localised view of cervical spine *(right images)* featuring anatomy completely different from the M-type tridactyls. Note the spacious spinal canal and posterior elements of vertebrae starting just above level of furcula *(yellow arrows)*. Note the upper part of the gastralia almost touching the spine. Isolated crushed vertebrae and subluxation are noted in all specimens.

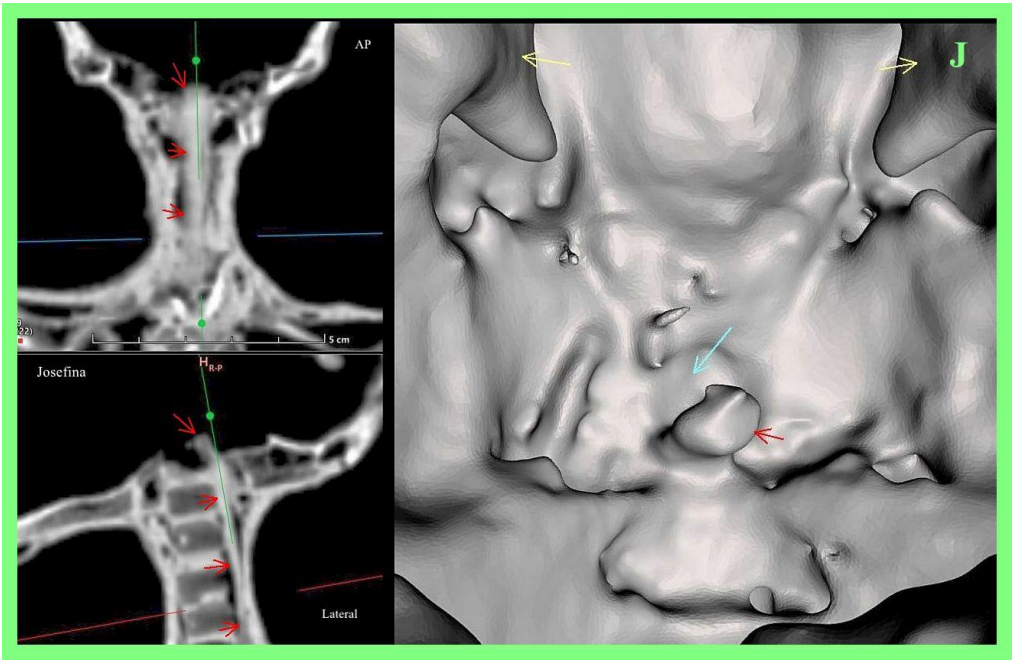

Figure 63: 2D coronal *(left upper)* and sagittal *(left lower)* CT scans showing cranio-vertebral junction of '***Josefina***' with virtual reality view inside the cranium looking downwards towards the foramen magnum *(right image)*. Note the remnant of spinal cord *(red arrow)* on the posterior surface of cervical vertebrae and its upper end protruding into the cranial cavity through the foramen magnum that is covered by soft tissue *(blue arrow)*. The skull base and bilateral otic capsules *(yellow arrows)* lying more anteriorly are also shown.

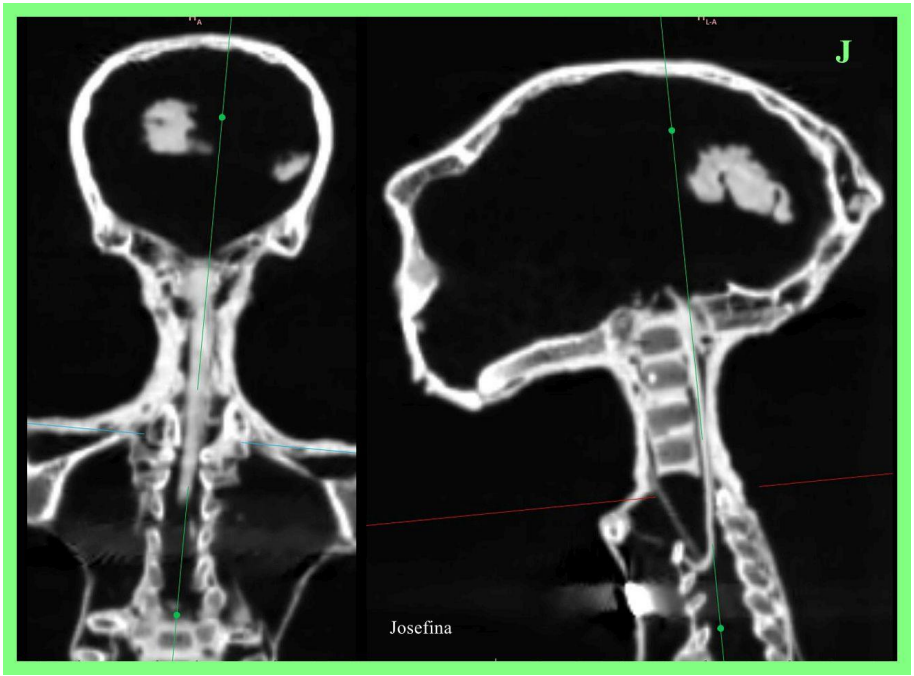

Figure 64: 2D coronal *(left image)* and sagittal *(right image)* CT scans showing cervical spinal cord of '***Josefina***' entering the spinal canal posteriorly at level above the furcula. It then loops anteriorly and become attached to the anterior process of the first thoracic vertebra, at the same time dividing into 2 parallel strands extending upwards and attaches to the skin at lower neck at midline.

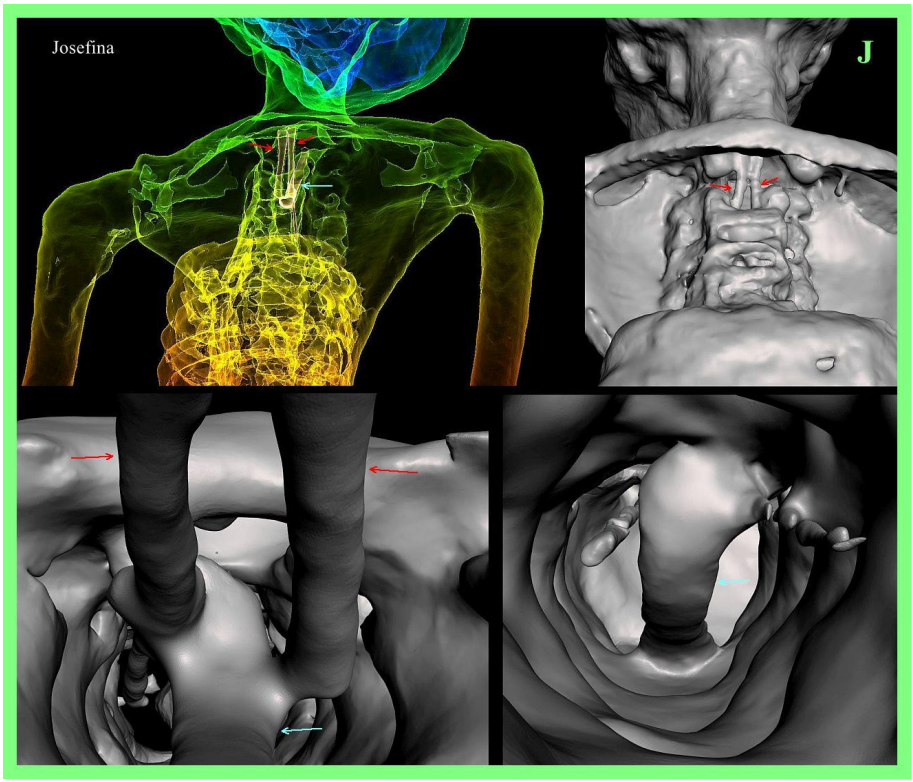

Figure 65: 3D CT in semi-transparency showing the spinal cord *(blue arrow)* in upper thoracic spine of '***Josefina***'. *(upper left image)* The spinal cord doubles back to form 2 parallel strands *(red arrow)* exiting the uppermost thoracic spine. *(top right image)* Antegrade *(bottom left image)* and retrograde virtual endoscopy *(bottom right image)* down the thoracic spinal canal showing the spinal cord *(blue arrow)* and the parallel strands *(red arrows)* exiting the anterior process of first thoracic vertebra.

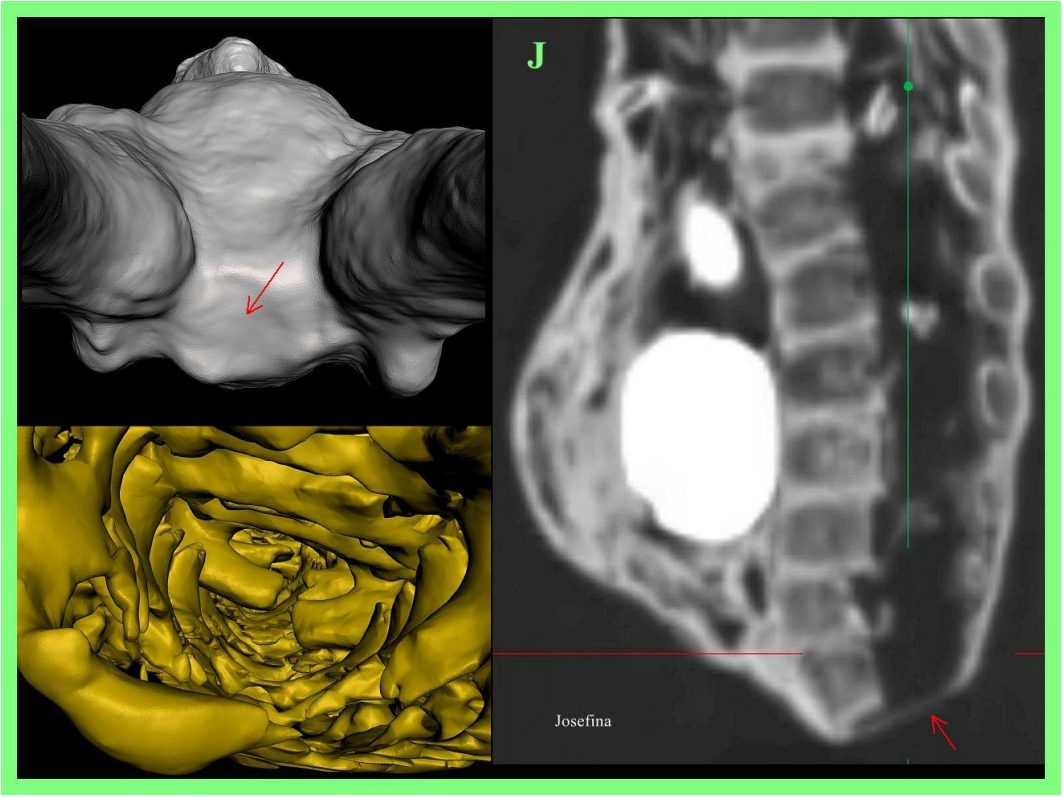

Figure 66: Virtual reality view of 3D CT of '***Josefina***' showing body surface *(left upper image)* and peeping into caudal end of spinal canal *(left lower image)* and 2D sagittal CT scan *(right image)* of lower end of spinal canal covered by thin skin *(red arrows)*.

SECTION 10: CONCLUSION

•The CT scan studies provide documentary proof that both ‘M-type’ and ‘J-type’ tridactyls show well-preserved, coherent, detailed, complex and integrated anatomy consistent with real biological entities that had been once living. This is further supported by evidence of skin and bone healing as reaction to injuries and metallic implants, bony remodelling, evidence of disease and degenerative bone changes and presence of brain remnant inside intact skull.

•The M-type and J-type tridactyls are completely different biological entities despite sharing common findings of bipedalism and tridactyl hands and feet.

•The M-type tridactyls resembles human to a large extent anatomically and could be considered hominids. The specimens include adult and children and are capable of bearing foetus.

•The J-type tridactyls show single forearm and leg bones instead of paired bones, single carpal and tarsal bones with tridactyls, unconventional anatomy in spine with enormous spinal canal ending abruptly. These combination of anatomical findings are unique and not documented in any other animals. They are ‘reptilians’ showing reptile-like skin and bear unique eggs, likely soft shelled but containing content or embryo exhibiting extremely high CT number (equivalent to metal). They have tubular rudimentary heart and great vessels on right side of body and unique orbits. ‘***Luisa***’ show different anatomy in the spine and hips as compared with ‘***Josefina***’ and ‘***Alberto***’ indicating different subspecies.

•All specimens including M-type and J-type showed evidences of significant trauma.

•There is evidence of superior medical and metallurgical technology, including metallic implants and bone grafting.

SECTION 11: FURTHER READINGS

Articles by same author in https://tridactyls.org

1) Comparative anatomy between human and M-type tridactyls.

2) Virtual autopsy of Nazca tridactyl mummy '***Maria***'.

3) The elongated skull of Nazca tridactyl mummy '***Montserrat***'.

4) Cause of death for tridactyl '***Montserrat***'.

5) Metallic implants in Peruvian Nazca tridactyl mummy '***Montserrat***'.

6) Virtual autopsy report of Nazca tridactyl mummy '***Sebastian***'.

ABOUT DR. FUNG

Dr. K H Fung is a retired radiologist with over 40 years of experience in diagnostic radiology. His special interests include 3D medical visualization, interventional radiology and neuro-intervention.

Dr. Fung is also an artist in the domain of intersection of art and science utilising his expertise in 3D medical visualization. Dr. Fung was the first place co-winner in the '2007 International Science & Engineering Visualization Challenge' organized by Science magazine and National Science Foundation (USA).

His artworks had been exhibited in museums in various countries including USA, Europe, China, Australia and Hong Kong.

He had current exhibits in 2025 in the Hong Kong Museum of Medical Sciences (featuring stereoscopic 3D and 4D medical imaging and art) and in Nina Park (featuring the Nina wood fossils collection) in Hong Kong.

Through his collaboration with Science Photo Library, his interdisciplinary artworks bridging art and science had been made available to various international renowned digital media, magazines, books, and journals.